Directional Information Flow and Applications

by

Shashank Prasanna

A Thesis Presented in Partial Fulfillment
of the Requirements for the Degree
Master of Science

Approved June 2011 by the
Graduate Supervisory Committee:

Konstantinos Tsakalis, Co-Chair
Leonidas Jassemidis, Co-Chair
Cihan Tepedelenlioglu

ARIZONA STATE UNIVERSITY

August 2011

ABSTRACT

In the late 1960s, Granger published a seminal study on causality in time series, using linear interdependencies and information transfer. Recent developments in the field of information theory have introduced new methods to investigate the transfer of information in dynamical systems. Using concepts from Chaos and Markov theory, much of these methods have evolved to capture non-linear relations and information flow between coupled dynamical systems with applications to fields like biomedical signal processing.

This thesis deals with the application of information theory to non-linear multivariate time series and develops measures of information flow to identify significant drivers and response (driven) components in networks of coupled sub-systems with variable coupling in strength and direction (uni- or bi-directional) for each connection. Transfer Entropy (TE) is used to quantify pairwise directional information. Four TE-based measures of information flow are proposed, namely TE Outflow (TEO), TE Inflow (TEI), TE Net flow (TEN), and Average TE flow (ATE).

First, the reliability of the information flow measures on models, with and without noise, is evaluated. The driver and response sub-systems in these models are identified. Second, these measures are applied to electroencephalographic (EEG) data from two patients with focal epilepsy. The analysis showed dominant directions of information flow between brain sites and identified the epileptogenic focus as the system component typically with the highest value for the proposed measures (for example, ATE). Statistical tests between pre-seizure (preictal) and post-seizure (postictal) information flow also showed a breakage of the driving of the brain by the focus after seizure onset.

The above findings shed light on the function of the epileptogenic focus and understanding of ictogenesis. It is expected that they will contribute to the diagnosis of epilepsy, for example by accurate identification of the epileptogenic focus from interictal periods, as well as the development of better seizure detection, prediction and control methods, for example by isolating pathologic areas of excessive information flow through electrical stimulation.

DEDICATION

To My Parents

ACKNOWLEDGMENTS

I am indebted to several people who have contributed directly or indirectly to this thesis. I am very thankful to my advisor Dr. Leonidas Iasemidis, for giving me the opportunity to work on this project. His encouragement, guidance and unreserved support made it possible for me to make a meaningful contribution to the field of Brain Dynamics.

I would like to thank Dr. Konstantinos Tsakalis and Dr. Cihan Tepedelenlioglu for serving as members of my thesis committee.

I extend special thanks to all my lab members at Brain Dynamics Lab, ASU. Dr. Ioannis Vlachos for patiently explaining to me the subtle concepts involved in the related topics and helping me shape my thesis and add rigor to my approach to problem solving, Balu Krishnan and Aaron Faith for answering all my queries promptly and helping me out whenever I needed help.

Last but never the least I would like to thank my parents for providing the encouragement and confidence that sustained me through rough times and Chaitra Hegde for standing by me always and giving me assurance when I needed it the most.

TABLE OF CONTENTS

Page

LIST OF TABLES

LIST OF FIGURES

Chapter 1

INTRODUCTION

1.1. Overview

Directional information flow is the key to understanding the interactions of dynamical system components. The identification of the driving and the response subsystem and estimation of the strength of interaction between such systems over time, especially when their structure is unknown, hold promise for the understanding of their dynamical behavior.

Commonly used tools for the estimation of linear dependencies between data series are the linear cross-correlation in the time domain and the cross-coherence in the frequency domain (Priestley, 1981). A mathematically more general and a statistical approach for the detection of linear and nonlinear interdependences between time series is the mutual information (MI) (Fraser & Swinney, 1986). It is a nonparametric and model-free measure that depends on the low and high order moments of a probability distribution. MI is however a symmetrical function and as a measure of Information flow cannot detect direction and hence causal relationships between two time series. An improvement on MI, which uses delayed time series for one of the time series, was a huge improvement toward the above goal but has its drawbacks; for example, its estimation requires a large number of data points, a strict requirement for experimental signals as they are typically noisy and nonstationary.

Granger (Granger, 1969) was one of the first to study the directional aspect of interactions, but assumed only linear dependencies. His approach has its roots to Norbert Wiener. Wiener (Wiener, 1956) introduced these concepts in

the context of linear regression models of stochastic processes. Granger causality was later extended to exploit nonlinearities in time series by applying local in time linear models, estimating statistical quantities from them, and then averaging over the entire dataset (Schiff, So, Chang, Burke, & Sauer, 1996); or by considering error reduction triggered by added variables in global nonlinear models (Liang, Ding, & Bressler, 2001).

Granger causality and its extensions were all model-based methods and, like all model-based analysis, they are plagued with modeling errors and modeling uncertainly. In order to overcome this hurdle, information-theory-based directional information flow and strength of coupling between complex systems/signals was introduced in Schreiber's seminal paper (Schreiber, 2000). This method was based on the study of transitional probabilities among states of systems under consideration, and it was named Transfer Entropy (TE).

In this thesis, TE and measures derived from TE are applied to multivariate time series data from a network of complex systems with varied couplings. Their applicability is demonstrated on models and electroencephalograph (EEG) data from epileptic patients.

1.2. Research Objectives

One of the main motivations for undertaking information flow analysis of multivariate time series data is because these are data commonly encountered in engineering applications including biomedical signals (EEG, EKG, EMG) and complex network of sensors. There are always observed interdependencies between various components of a complex system and, for systems where the model structure is unknown, time series analysis offers the only window to the

system's working behavior. The information theoretic approach to detecting nonlinear relations between time series offers significant advantages over other linear causal approaches. Also, TE being a directional measure, it captures the direction of coupling in addition to the coupling's strength.

The primary objective of this thesis has been to formulate a strong framework for the analysis of such multivariate time series data recorded from a coupled system, and to empirically validate its ability to detect the strongest drivers present in the system by existing and new measures we developed that involve TE.

We also present results on the application of these methodologies to electroencephalographic (EEG) time series from epileptic patients with focal epilepsy, which motivated our efforts towards the culmination of this work. First, measures for identifying drivers in a system were developed. Second, these measures were applied to EEG data to observe dynamical changes prior to a seizure in the temporal (time) and spatial (brain's) domain. These changes were further utilized to address the still unresolved problem of epileptogenic focus localization. We address this particular problem by looking at a seizure as a connectivity-breaking event of the information flow from the focus to other brain sites. The above findings shed light on the function of the epileptogenic focus and understanding of ictogenesis (genesis of epileptic seizures). The performance of the measures we developed was evaluated on the EEG from for two patients over several days of recording.

1.3. Thesis Organization

This thesis is further organized in chapters as follows. Chapter 2 outlines a brief description of dynamical systems and chaos theory, and introduces information flow and several existing measures for analysis of time series from coupled chaotic systems. Chapter 3 introduces TE as a measure for directional information flow and discusses two methods for its estimation. Based on TE, measures to detect directional information flow in a network of coupled systems are then introduced. Chapter 4 uses the methods discussed in Chapter 3 and applies them to multivariate time series from coupled mathematical models of nonlinear oscillators. The results are also discussed with respect to the measures' robustness to noise. Chapter 5 demonstrates the application of the methods developed in Chapter 3 to electroencephalographic (EEG) data from two patients with focal epilepsy. The results during preictal, ictal and postictal periods are presented along with their possible use for seizure prediction and detection. In Chapter 6, conclusions are presented and future work is discussed.

Chapter 2

INFORMATION FLOW IN DYNAMICAL SYSTEMS

2.1. Dynamical Systems and Chaos

Chaos theory studies the behavior of nonlinear dynamical systems that are highly sensitive to initial conditions. Differential equations have been used to model physical systems to find out how they may behave temporally under different than the experimental conditions and thus try to predict their future dynamics. As the order and degree of the modeled systems get higher, analytical solutions become impossible to compute. Nonlinear systems for which analytical solutions were found exhibited regular motions, i.e. if a solution was bounded, the system either settled in a steady state or in a periodic motion. Around 1975, a third kind of motion was observed which was erratic. This type of motion was termed chaos, and the theory to explain such systems came to be known as Chaos theory.

A system is said to be in an unstable steady state if small changes makes the system evolve away from the steady state. For example a cone resting on its apex can be balanced at just one particular point. But if the cone is perturbed it falls to the ground which is a stable (static or dynamic) state. A system which experiences more complicated steady states, in the sense that there is no particular region in the state space the system may eventually rest to or stabilize in is said to be a chaotic system. Even though nearby points in the state space of a chaotic system move away from each other, a steady chaotic state can dynamically be defined as stable if the system always moves (randomly, according to a deterministic probability distribution) within it and never escapes from it under a small bounded perturbation (chaotic attractor).

The existence of such systems was known for some time but they were first described mathematically by Lorenz in his seminal paper in 1963. He presented a system of 3 coupled differential equations that could behave chaotically depending on the value of a parameter. He observed that a small change in the initial conditions led to large change in the corresponding trajectories. This led him to his now famous speculation that a butterfly flapping its wings in Brazil (that is, a small change in the initial conditions in the atmosphere) might cause a tornado in Texas (which is a long-term unpredictable phenomenon).

Chaotic motion is complex. It is intuitive to expect the systems in nature that exhibit chaos to be complex too. Hence we expect, the larger the number of system state variables, the more complex the system and hence larger the probability that the system exhibits chaos. For example, chaos can be exhibited only by systems with dimension of at least 3.

For autonomous differential equations on a real line all bounded solutions converge to a fixed point. For two dimensional autonomous differential equations, the solutions can either converge to a fixed or a periodic orbit also called a limit cycle. Hence chaos cannot exist in such system. This is given by the Poincare - Bendixson theorem. For a system of autonomous differential equations to exhibit chaos, the dimension of the system should be at least 3. Many systems of dimension 3 have been described which exhibit chaotic motion. Examples include the Lorenz and Rossler systems. Maps can be classified into invertible and non-invertible. A map M is said to be invertible if there exists a unique x_n for every $x_n + 1$. In other words the mapping is one to one. Hence x_n is given by

$$x_n = M^{-1}(x_{n+1}) \tag{2.1}$$

Non invertible maps are those for which M^{-1} cannot be defined as the system can evolve to the same state from two different states. For invertible maps chaos can exist only for dimensions two and above (the third dimension is implicit, due to “discretization”, because the system is a map). But for non-invertible maps chaos can exist even in one dimensional maps. Examples include logistic map, tent map (Williams, 1997).

The properties of chaotic systems are explained below.

1.) The system is deterministic: Even though chaotic system exhibit random like behavior, they are still deterministic systems. If the initial conditions are known precisely then it is possible to predict the future behavior of the system. However in real systems, the initial conditions are never known precisely, which leads to random like behavior of chaotic systems.

2.) The system is nonlinear: For a system to exhibit chaotic behavior, there has to be an element of nonlinearity. Perfectly linear system can never exhibit chaos. However even a little nonlinearity can induce chaos. For example, the Henon map is barely nonlinear in the sense that it just has an x^2 term and all the other terms are linear. But the map exhibits chaotic behavior.

3.) The system exhibits sensitivity to initial conditions: This is the most important characteristic of chaotic systems. It states that any two initial conditions diverge exponentially as the systems evolves with time. Hence, any small change in the initial conditions takes the system in a completely different trajectory. There are always errors and the initial conditions of a system are not known precisely. Hence predictions after a

certain time become impossible as the error in the initial conditions is amplified exponentially.

4.) The system is bounded: This is a condition put on the system in order to eliminate trivial cases. If the orbits go to infinity, it is very easy for distances to diverge to infinity. For example consider a system $\frac{dx}{dt} = x$, the error Δx is given by e^t which diverges exponentially. However the system is not chaotic as it's not bounded.

2.2. State Space Representation and State Space Reconstruction

State space, also referred to as Phase space, is a vector space in which all possible states of a system are represented with a unique point or set of points (vectors). The rank of this space gives the necessary number of degrees of freedom or variables the system may have. The succession of points in the state space is representative of how the system evolves over time.

Often, as a part of an engineering experiment, one measures data (e.g. from sensors) over time, thus ending up with a time series. This time series data can be, for instance, from a single EEG channel that measures the electric potential of millions of firing neurons, or from a seismograph, which measures ground motion to detect tremors prior to, during and after an earthquake. For real-world systems of such complexity as the human brain or the seismic activity of the earth, an accurate model representing the dynamics of the system is not known. We have to rely on the analysis of time series to understand the underlying dynamics of such systems.

The complexity of modeling nonlinear systems must not be underestimated. Research in nonlinear dynamical analysis of time series is a

relatively new field of study and much progress has been seen in generating reliable models in recent times. The approach we discuss in this thesis is based on the method of the delay-coordinate embedding for the reconstruction of the state space of an unknown system, developed by Takens (Takens, 1981). The embedding method has been proven useful, particularly for time series generated from low-dimensional, deterministic or mostly deterministic dynamical systems. For situations where the dynamical invariant set (steady state) responsible for the behavior observed in the measured time series is low-dimensional, and the influence of noise is relatively small, the delay-coordinate embedding method can yield reliable information essential for understanding the underlying dynamical system. The method has been applied to several fields in engineering and has been a favorite approach in analyzing epileptic EEG signals for seizure prediction (L. D. Iasemidis et al., 2003). There have been several works that start with the delay coordinate embedding technique and are then applied to dynamical systems with chaotic attractors (Abarbanel, 1996)(Kantz, Schreiber, & Mackay, 1997).

The underlying dynamics of any system is in principle represented by a mathematical model involving a set of differential equations. The dynamical variables of all first order equations constitute the state space and the number of such variables is the dimension of the state space, usually denoted by m. It occurs that the asymptotic evolution of a system (steady state) usually is well defined in a finite dimensional state space. The delay coordinate embedding technique (Takens, 1981) provides an accepted practical solution to determining this approximate behavior. In general Takens' embedding theorem guarantees that a topological equivalence of the state space of the intrinsic unknown

dynamical system can be reconstructed from the time series generated by measurement of the system's variables values over time, subsequently based on which characteristics of the dynamical invariant set of the steady state can be estimated.

Taken's embedding theorem is explained in simple terms as follows. Given a measured time series $\boldsymbol{x}_i(t)$, the time-delay vectors $\boldsymbol{X}_i(t)$ are a one-to-one representation of the state vectors (points in the state space A) for m sufficiently large.

$$\boldsymbol{X}_i(n) = \{\boldsymbol{x}_i(n), \boldsymbol{x}_i(n + \tau), \ldots, \boldsymbol{x}_i[n + (m-1)\tau]\} \tag{2.2}$$

The delay time τ and the embedding dimension m are the important parameters to be considered for the state space reconstruction.

Delay time τ*.* To select the delay time, we must first note that any discrete-time map can be regarded as arising from the section of a Poincare surface with the continuous time series (Ott, 2002). Thus, one iteration of the map corresponds to roughly one period of oscillation of the continuous-time signal $x(t)$, which, for chaotic systems, is approximately the decay time of the autocorrelation of $x(t)$. As an empirical rule, the delay time can be chosen to be $\tau = 1$ for chaotic time series from discrete-time maps.

In order for the time-delayed components $\boldsymbol{x}_i[n + (p-1)\tau]$ to serve as independent variables, the delay time has to be chosen carefully. If the delay time is too small, then adjacent components $\boldsymbol{x}_i(n), \boldsymbol{x}_i(n + \tau)$ will be too much correlated to be considered as independent coordinates. On the other hand, if the delay is too large, adjacent components become too uncorrelated (almost independent) and cannot be part of a system that supposedly generated them. One can examine the autocorrelation function of $x(t)$ and decide a proper delay

time (Theiler, 1986). In particular, it is suggested (Rapp, Albano, & Mees, 1988; Schreiber, 2000) that one can choose τ when the autocorrelation drops to $1/e$ times the initial value.

The second method selects τ as the one equal to the first local minimum of the time-delayed mutual information (Fraser & Swinney, 1986). Mutual information is a measure of mutual dependence (linear or non-linear) between two variables quantifying the reduction of the uncertainty about one variable when we know the other. The mutual information of two variables X and Y is defined as

$$I(X,Y) = \int_{S_X}\int_{S_Y} p(x,y)\ln\left(\frac{p(x,y)}{p(x)p(y)}\right)dxdy \tag{2.3}$$

where $p(x,y)$ is the joint probability density function (pdf) of X and Y , $p(x)$ and $p(y)$ are the marginal pdfs of X and Y respectively, and S_X and S_Y are the support sets of the two random variables (the sets where $p(x) > 0$ and $p(y) > 0$). Time-delayed mutual information is the mutual information of a single variable at different time indices

$$I(\tau) = I(X_n, X_{n-r}) \tag{2.4}$$

There exist various alternative empirical methods for choosing a proper delay time [Liebert & Schuster, 1989; Liebert et al., 1991; Buzug & Pfister, 1992; Kember & Fowler, 1993; Rosenstein et al., 1994], which all yield similar results.

Embedding dimension m. In order to have a close representation of the true dynamical system, the embedding dimension m should be sufficiently large (Takens, 1981). Takens theorm provides a lower bound for m. In particular, suppose the dynamical invariant set lies in a d-dimensional manifold (or subspace) in the state space. Then, if $m > 2d$, the m-dimensional reconstructed

vectors $u(t)$ have a one-to-one correspondence to the vectors of the true dynamical system.

The reconstructed system obtained by the time-delay vectors should be topologically equivalent to the original as long as $m \geq 2d + 1$ where d is the box-counting dimension of the original system.. Among the approaches for the selection of m, we chose the most popular method of false nearest neighbors (FNN) and present it briefly below (Kennel, Brown, & Abarbanel, 1992). For a small , the reconstructed points are badly projected to the state space, However, we would like to have a reconstructed state space of the smallest embedding dimension m that unfolds the attractor. This idea is implemented as follows. For each point $\boldsymbol{x}_i^n$ in the m-dimensional reconstructed state space, its nearest neighbor $\boldsymbol{x}_{i(1)}^m$ is located and their distance is calculated, $d\left(\boldsymbol{x}_i^m, \boldsymbol{x}_{i(1)}^m\right) = \left\|\boldsymbol{x}_i^m - \boldsymbol{x}_{i(1)}^m\right\|$. The metric used is usually the maximum norm, or the Euclidean norm. The dimension of the reconstructed state space is augmented by 1 and the new distance of these vectors is calculated, $d\left(\boldsymbol{x}_i^{m+1}, \boldsymbol{x}_i^{m+1}\right) = \left\|\boldsymbol{x}_i^{m+1} - \boldsymbol{x}_{i(1)}^{m+1}\right\|$

If the ratio of the two distances exceeds a predefined tolerance threshold A the two neighbors are classified as false neighbors, i.e.

$$A_i(m) = \frac{d\left(\boldsymbol{x}_i^{m+1}, \boldsymbol{x}_{i(1)}^{m+1}\right)}{d\left(\boldsymbol{x}_i^m, \boldsymbol{x}_{i(1)}^m\right)} > A \tag{2.5}$$

The criterion that the embedding dimension m is high enough to unfold the attractor is that the percentage of points for which $A_i(m) > A$, is essentially zero (usually set to 1% of the total number of points / vectors).The selection of A should be large enough to allow for exponential divergence (Kennel et al., 1992). Empirically, a good and often used value for A is 2.

The invariant quantities of a steady state of the original system (dimensions, Lyapunov exponents, etc) can be estimated in the reconstructed state space as we will see when we discuss application of these measures to time series generated from models and physical systems.

2.3. Discrete Systems: Henon Chaotic Map

The Henon map (Hénon, 1976) is a discrete-time dynamical system. It is one of the most studied examples of dynamical systems that exhibit chaotic behavior. It is given as

(2.6)

The map depends on two parameters, and , which for the canonical Henon map have values of and for the map to produce chaotic behavior. This map is shown in Figure 2.1.

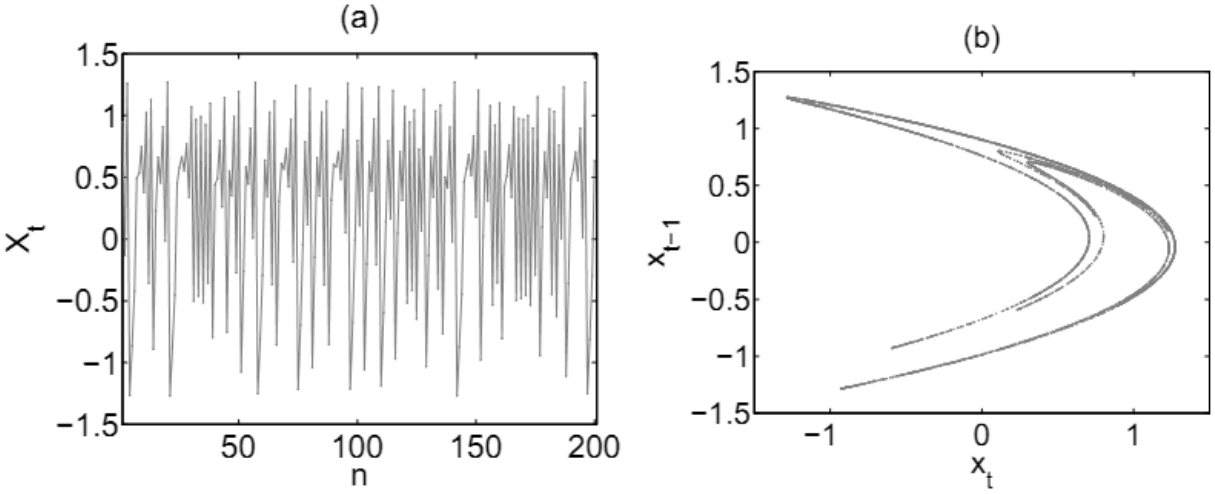

Figure 2.1: (a) One realization of the Henon map over time with n = 200. (b) The strange attractor of the Henon map in the state space.

2.4. Continuous Systems: Rossler Chaotic Attractor

The Rossler attractor (Rössler, 1976) is given by the differential equations

$$\dot{x} = -y - z, \qquad \dot{y} = x + 0.15y, \qquad (2.7)$$

$$\dot{z} = 0.2 + xz - 10z$$

with a sampling time of 0.1. In Figure 2.2, the time series segments for x and y variables and the attractor of the system are shown. Figure 2(c) shows the projection of the attractor on the $x - y$ plane and Figure 2(d) shows the plot of x_n versus x_{n-14} delay representation. The shape in Figure 2(d) is a distorted version of the shape in Figure 3.2(c). Despite the distortion of the shape, it can be proven that the invariances in dynamics (e.g. dimension, Lyapunov exponents) are preserved.

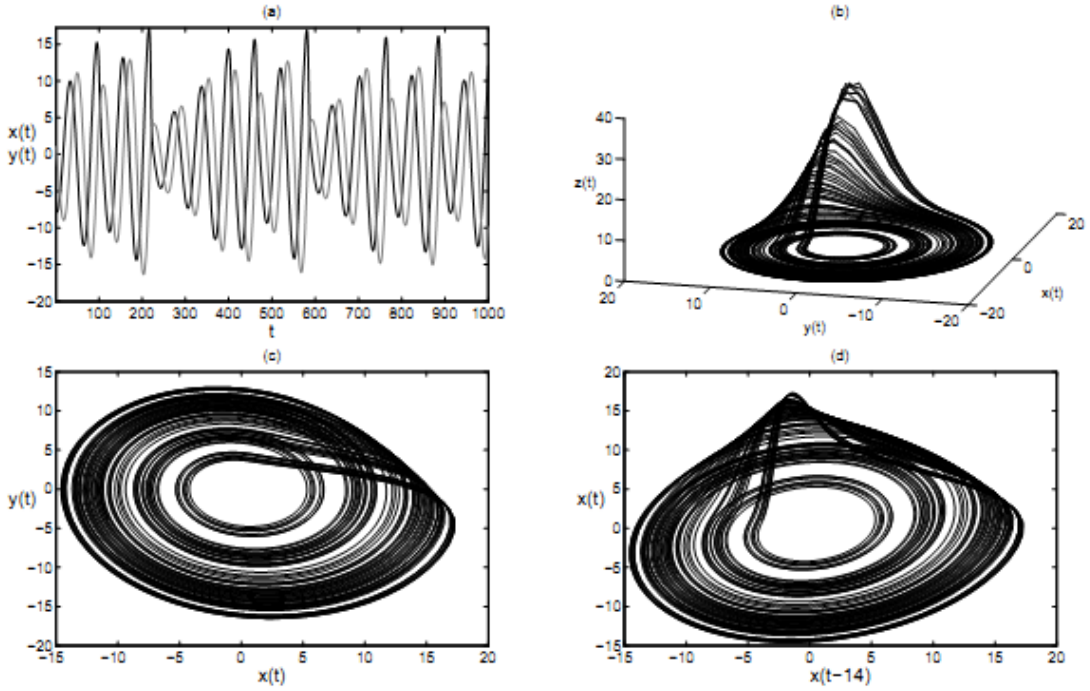

Figure 2.2: Rossler system in the reconstructed state space: (a) time series of the x_n (black line) and y_n (grey line), (b) the attractor, (c) scatter plot of (x_n, y_n), (d) scatter plot of (x_n, x_{n-14})

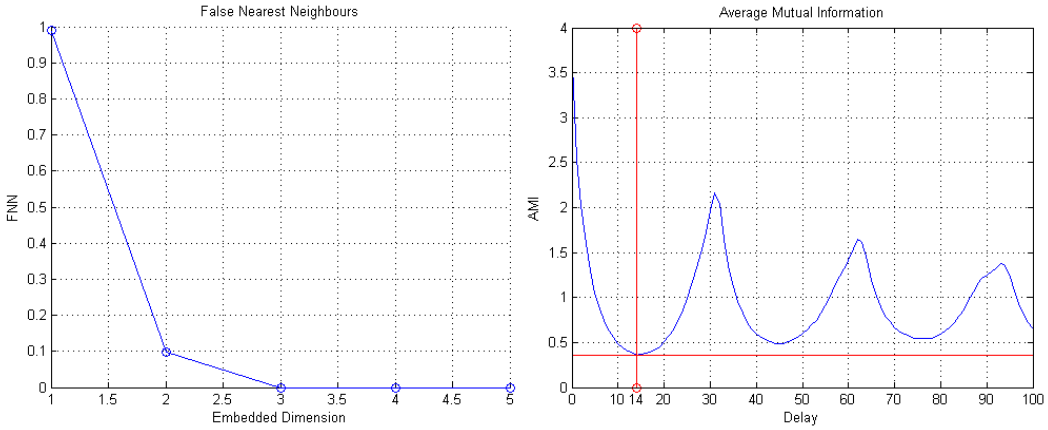

(a) (b)

Figure 2.3: Rossler attractor. (a) False Nearest Neighbors for $m = 1,..,5$ and (b) Time Delay Mutual Information (its first minimum is marked with red cross-hair).

As evident from Figure 3, the Rossler attractor was reconstructed by choosing the embedding dimension m using the False Nearest Neighbor method and the Time Delay $\tau = 14$ from the first minimum of the Time Delay Mutual Information plot.

2.5. Measures of Directional Information Flow

The interaction or coupling between variables of a system is a developing area of nonlinear dynamics and time series analysis (Hlavackova-Schindler, Palus, Vejmelka, & Bhattacharya, 2007). The detection and characterization of interdependence among interacting components of complex systems can give information about their function and a better understanding of the underlying system dynamics. Information flow is an essential feature of many complex physical phenomena, such as climatic processes (Smith, Wigley, & Santer,

2003), brain function (Kaminski & Blinowska, 1991) and other processes in many other fields.

In this section the most commonly used measures of information flow are reviewed and the most promising methods are considered for application to models and information flow in the brain of epileptic patients.

Granger Causality

For a given set of time series observations, it is essential to assess whether they originate from coupled or decoupled systems, detect the hidden causal dependencies between them, and understand which system is the driver and which is the driven. Granger causality (Granger, 1969) was the leading approach for a long time inferring the direction of interactions. Granger investigated the dependencies between time series and whether one time series is useful in forecasting another. Granger causality assumes linearity of the models for the predictability of time series.

Granger causality estimates the information flow between two time series using the methodology of prediction. For any two time series X and Y, X 'causes' Y if the prediction of future values of Y can be improved by using past values of X too. Consider two time series $x(n)$ and $y(n)$ which are the results of two processes X and . Modeling X and Y using pth order autoregressive models we can write

$$x(n) = \sum_{k=1}^{p} a_{ik} x(n-k) + \mu_1(n) \tag{2.8}$$

$$y(n) = \sum_{k=1}^{p} b_{ik} y(n-k) + \nu_1(n) \tag{2.9}$$

where a_{1k} and b_{1k} are the autoregressive coefficient and μ_1 and ν_1 are the prediction error for the process X and Y respectively. Incorporating the information of process Y in determining the future values of process X and vice versa, we get the new bivariate autoregressive models as

$$x(n) = \sum_{k=1}^{p} a_{ik} x(n-k) + \sum_{k=1}^{p} c_{ik} y(n-k) + \mu_2(n) \tag{2.10}$$

$$y(n) = \sum_{k=1}^{p} b_{ik} y(n-k) + \sum_{k=1}^{p} d_{ik} x(n-k) + \nu_2(n) \tag{2.11}$$

where μ_2 and ν_2 are the new prediction error for the process X and Y respectively. Prediction of future values of x is dependent on the past values of both x and y. Similarly prediction of future values of y is dependent on past values of y and x. Let $\Sigma_{x\backslash x}$, $\Sigma_{y\backslash y}$, $\Sigma_{\mathrm{x\backslash(x,y)}}$,$\Sigma_{\mathrm{y\backslash(y,x)}}$ be the variance of the sequence $\mu_1(n)$, $\nu_1(n)$, $\mu_2(n)$, $\nu_2(n)$ respectively.

If X has causal influence on Y, then $\Sigma_{\mathrm{y\backslash(y,x)}}$ should be less than $\Sigma_{y\backslash y}$, and similarly if there is information flow from Y to X, then variance $\Sigma_{\mathrm{x\backslash(x,y)}}$ should be lower than $\Sigma_{x\backslash x}$. The idea is that, the extra information available in y about x is included in the autoregressive modeling to provide better prediction of the future values of x. Geweke et al. (Geweke, 1982) defined the Granger causality from Y to X as

$$F_{Y\to X} = \ln\left(\frac{\Sigma_{x\setminus(x,y)}}{\Sigma_{x\setminus x}}\right) \tag{2.12}$$

$$F_{X\to Y} = \ln\left(\frac{\Sigma_{y\setminus(y,x)}}{\Sigma_{y\setminus y}}\right) \tag{2.13}$$

$$F_{X,Y} = \max\left(F_{Y\to X}, F_{X\to Y}\right) \tag{2.14}$$

Depending on the values of $F_{X,Y}$ we determine the strength of directional interaction between processes X and Y. It has to be noted that Granger causality might not be a true indication of causality when two processes (X, Y) might be both controlled by a third process (Z) and, depending on the strength of interaction, Granger causality may not detect the causal relation existing between X and Y, or may falsely detect causality between X and Y when Z is driving both X and Y.

Many measures have been developed based on the concept of Granger causality and extended it in order to also incorporate nonlinear relationships between the involved time series. The recently developed measures of interaction go beyond the standard cross-correlation and exploit nonlinear properties of dynamical systems. These measures can be divided in three main categories

I. Event synchronization (Rosenblum & Pikovsky,) (Smirnov & Bezruchko, 2003),
II. Reconstruction of the state spaces (Mormann et al., 2003) (Feldmann & Bhattacharya, 2004)
III. Information theory (Schreiber, 2000) (Paluš, Komárek, Hrnčíř, & Štěrbová, 2001)

The measures based on Information theory make no assumptions on the system dynamics whereas event synchronization measures assume strong oscillatory behavior or distinct event occurrences, and the state space methods require local dynamics to be preserved in neighborhoods of reconstructed points. We will now present a brief discussion of some of these methods, and their application in models and EEG data is left for subsequent chapters. Emphasis will be made on the Information Theory measures which yielded promising results for the data and the nature of applications under our consideration.

Let $\{x_n\}$ and $\{y_n\}$ be two univariate time series obtained from dynamical systems X and Y for $n = 1, \ldots\ldots, N$. Let also assume there exists a unidirectional coupling and X is the driver system and Y is the driven system. The notation $X \rightarrow Y$ is used in order to indicate the effect of X on Y, while $Y \rightarrow X$ is indicating the inverse. Moreover, all the measures are defined in order to allow for different parameters in the embedding of the corresponding variables X and Y of the time series. Let k and l be the embedding dimensions, and τ_x and τ_y the delays, for the two systems / time series, respectively.

Transfer entropy

Transfer entropy (TE) is an information theoretic measure which takes into account the dynamics of information transport and detects the directed exchange of information between two systems. As defined by Schreiber (Schreiber, 2000), TE quantifies the information flow from X to Y by the amount of information we obtain about the future position of Y in the state space by observing the present state of X and Y. The concept of transfer entropy extends the Shannon entropy for transition probabilities and quantifies how the

conditioning on X changes the transition probabilities of Y. It has been shown that transfer entropy $TE_{X\to Y}$ is the exact equivalent to the conditional mutual information $I(y_{n+\tau}|x_n, y_n)$ (Hlavackova-Schindler et al., 2007). TE is defined here in accordance with the state space nomenclature as

$$TE_{Y\to X} = \sum p\left(x_{n+1}, x_n^{(k)}, y_n^{(l)}\right) \log\left(\frac{p\left(x_{n+1}\middle| x_n^{(k)}, y_n^{(l)}\right)}{p\left(x_{n+1}\middle| x_n^{(k)}\right)}\right) \tag{2.15}$$

where $x_n^{(k)}$and $y_n^{(l)}$represent the embedding vectors with an embedding dimension specified as superscript.

TE can also be defined in terms of entropies as

$$\begin{aligned} TE_{Y\to X} &= I\left(x_{n+1}, y_n^{(l)}\middle| x_n^{(k)}\right) \\ &= H\left(x_{n+1}\middle| x_n^{(k)}\right) - H\left(x_{n+1}|x_n^{(k)}, y_n^{(l)}\right) \end{aligned} \tag{2.16}$$

where $H\left(x_{n+1}\middle| x_n^{(k)}\right)$ is the information gained about the future state x_{n+1} by using the information from $x_n^{(k)}$ and $H\left(x_{n+1}|x_n^{(k)}, y_n^{(l)}\right)$ is the information gained about the future state by using the information from $y_n^{(l)}$ in addition to $H\left(x_{n+1}|x_n^{(k)}, y_n^{(l)}\right)$. Thus, $TE_{Y\to X}$ is the additional information gained from process Y about the future state of the process X, and therefore it can be seen as the information flow from the process Y to process X. Equation 2.16 also implies that when the processes X and Y are independent, the value of $TE_{Y\to X}$ is zero.

Since we assume X to be continuous, and possibly a vector-valued random variable, for a fixed small r, the $TE_{X\to Y}$ can be estimated in terms of the correlation sum as

$$TE_{Y\to X} = \log\left(\frac{C_r\left(x_{n+1}, x_n^{(k)}, y_n^{(l)}\right) C_r\left(x_n^{(k)}\right)}{C_r\left(x_{n+1}, x_n^{(k)}\right) C_r\left(x_n^{(k)}, y_n^{(l)}\right)}\right) \tag{2.17}$$

In Chapter 3 we shall see another method for estimation of TE using the nearest neighbors' method to calculate mutual information in Equation 2.16

Chapter 3

METHODS OF ESTIMATION OF INFORMATION FLOW

3.1. Transfer Entropy (TE) Estimation Methods

In chapter 2, we discussed time series analysis and various approaches to state space reconstruction, presented examples of mathematical models of chaos, and explained the basics behind Transfer of Entropy between time series. In this chapter we will detail the method of Transfer Entropy to detect directional information flow in coupled dynamical systems and employ it to detect and localize driving and driven systems from multivariate time series obtained from a network of coupled systems with unknown coupling strength and direction.

We shall also discuss two different methods for the estimation of Transfer Entropy and compare them qualitatively for merits and demerits. The methods differ in the involved entropy and probability densities estimation in the embedding state space.

Consider a k^{th} order Markov process (Bharucha-Reid, 1997) described by

$$P\ (X_{n+1}|X_n, X_{(n-1)} \dots\dots\dots X_{n-k+1}) = P\ (X_{n+1}|X_n, X_{(n-1)} \dots\dots\dots X_{n-k}) \tag{3.1}$$

where P is the conditional probability of a random process X being in state X_{n+1} at time $n+1$ upon the past k states $\left[X_n, X_{(n-1)} \dots\dots\dots X_{n-k+1}\right] \triangleq X_n^{(k)}$ of the system. The Markov dependence described in Equation 3.1 can be extended to the case of Markov interdependence of two random processes X and Y as

$$P\left(X_{n+1}\middle|X_n^{(k)}\right) = P\left(X_{n+1}\middle|X_n^{(k)}, Y_n^{l}\right) \tag{3.2}$$

where Y_n^l are the past l states of the second random process Y. This generalized Markov property implies that the state X_{n+1} of the process X depends on the past

k states of the process X and on the past l states of the process Y. If the process X also depends on the past states (values) of process Y, the divergence between Equations 3.1 and 3.2 can be quantified using the Kullback-Leibler measure (Quiroga, Arnhold, Lehnertz, & Grassberger, 2000), where $P\ (X_{n+1}|X_n^k)$ is the hypothesized (a priori) transition probability and $P\ (X_{n+1}|X_n^k\ , Y_n^l)$ is the true underlying transition probability of the system. It can then easily be shown that the Kullback-Leibler measure quantifies the transfer of entropy from the driving process Y to the driven process X, and it is given by Equation 2.15

The values of the parameters k and l are the orders of the Markov process for the two coupled processes X and Y respectively.

A simple manipulation of Equation 3.3 permits a decomposition of the transfer entropy in terms of conditional entropies (Paulus, Komarek, Prochazka, Hrncir, & Sterbova, 2001) and justifies the use of TE as a measure of information flow from Y to X in Equation 2.16

3.1.1. Estimation of Transfer Entropy: Correlation Integral Approach

The first method for estimation of Transfer Entropy from the correlation integral was detailed in Chapter 2. From Schreiber (Schreiber, 2000), Transfer Entropy from $Y \rightarrow X$ is defined as in Equation 3.3, where the probabilities are calculated using the correlation integral. For discrete systems, the correlation integral can be approximated by the correlation sum defined as

$$C_r\left(\boldsymbol{x}^{(\boldsymbol{k})}\right) = \frac{2}{n_{pairs}} \sum_{i=k}^{n} \sum_{i<j-W} \Theta\left(r - \left\| x_i^{(k)} - x_j^{(k)} \right\|\right) \tag{3.3}$$

Here n is the number of time points, k is the embedding dimension for x, W is the Theiler window (Theiler, 1986), $n_{pairs} = (n-k+1)(n-k-W+1)$, r is a

threshold value and $\|\cdot\|$ is a distance norm. (Any norm can be used although maximum norm is considered for computational reasons.) $\Theta(\cdot)$ is the Heaviside step function. W is used to avoid spurious correlations which creeps in due to neighbors being very close in time (high sampling frequency) due to continuity of the signal in the time domain and not to its dynamics.

For small radius r , the entropy of a variable X can be estimated in terms of the correlation sum as

$$H(X) \simeq \ln C\left(\boldsymbol{x}^{(\boldsymbol{k})}\right) + k \ln r \tag{3.4}$$

This approximation allows us to define $TE_{Y\to X}$ as

$$\begin{aligned} TE_{Y\to X} = & -H\left(x_{n+1}, x_n^{(k)}, y_n^{(l)}\right) - H\left(x_n^{(k)}\right) \\ & + H\left(x_{n+1}, x_n^{(k)}\right) + H\left(x_n^{(k)}, y_n^{(l)}\right) \end{aligned} \tag{3.5}$$

which gives us Equation 2.17

3.1.2. Estimation of Transfer Entropy: K-nearest neighbor Approach

This method differs from the previous method in the estimation of the mutual information. The calculation of $H(X)$ in Equation 3.7 is based on the K-neighbor distances.

The joint entropy for $H\left(x_{n+1}, x_n^{(k)}, y_n^{(l)}\right)$ from Equation 3.5, is estimated by

$$_{+1}, x_n^{(k)}, y_n^{(l)}\Big) = -\psi(k) + \psi(N) + \log(c_k c_l c_1) + \frac{k+l+1}{N}\sum_{i=1}^{N} \log \epsilon(i) \tag{3.6}$$

while the entropy $H\left(x_n^{(k)}\right)$ (and accordingly for the other two entropies in Equation 3.5) is estimated by

$$H\left(x_n^{(k)}\right) = \frac{1}{N}\sum_{i-1}^{N}\psi\left[n_{x^{(k)}}(i)\right] + \psi(N) + \log(c_k) + \frac{k}{N}\sum_{i=1}^{N}\log\epsilon(i) \tag{3.7}$$

The space that $(x_n^{(k)})$ evolves is considered a projection from the higher-dimensional space where $(x_{n+1}, x_n^{(k)}, y_n^{(l)})$ evolves.

with $n_{x^{(k)}}$ is the number of points whose distance from the ith point of $x_n^{(k)}$ is less than $\frac{\epsilon(i)}{2}$ plus one, $\psi(x)$ is the digamma function $[\psi(x) = \frac{d}{dx}\log\Gamma(x) = \frac{\Gamma'(x)}{\Gamma(x)}]$ and c_k is the volume of the d-dimensional unit cube, using the maximum norm as the distance metric. Since we know Transfer Entropy is equivalent to the normalized Conditional Mutual Information (Hlavackova-Schindler et al., 2007) we have from Equation 2.16 where the mutual information H is calculated by Equation 3.6 and Equation 3.7 instead of using the correlation integral.

3.2. Optimal Data structure and an Efficient Algorithm to compute TE

The computation of $TE_{Y\to X}$ (Equation 3.5) is a computationally intensive task. The key step in the estimation of TE involves estimation of the correlation integral (Equation 3.3). Computation of $C_r\left(\boldsymbol{x}^{(k)}\right)$ takes most of the computation time, because it involves a nearest neighbor search in a $k + l$ embedding space. With the amount of data at hand (over 85 hours of data for two patients including interictal and ictal data) an efficient algorithm was essential.

An important step in the computation of correlation sum is to find the maximum numbers of neighbors for a given point in a k-embedded space. This directly affects the optimality of the data structure used to hold the embedded

data. A quick intuitive approach (commonly referred to as the brute force method) is to iteratively go through every single node in linked list for a reference node, simultaneously computing the distance between the current node and the reference node and keeping in memory the number of neighbors for a given reference node. Although this method is simple in conception, it suffers from the biggest cost with respect to time complexity. Every node is traversed at most N times, where N is the total number of data points in the segment of analysis (2048 in the EEG analysis). This yields an asymptotic polynomial time complexity of $O(N^2)$. Literature in cost of algorithms (Cormen, 2001) tells us that this is inefficient and too computational intensive. We need to use a data structure that has quick retrieval in order to reduce the time complexity for the nearest neighbor search. K-d tree data structure is employed for this purpose.

K-d tree (short for k-dimensional tree) is a space-partitioning data structure for organizing points in a k-dimensional space. K-d trees are particularly useful for applications involving searches in multidimensional spaces. K-d trees are a special case of binary space partitioning trees. In this thesis we shall refrain going into the details of the data structure with regard to its construction. For more details the reader can refer to (Bentley & Friedman, 1979; Eastman, 1982; Friedman, Baskett, & Shustek, 1975; Friedman, Bentley, & Finkel, 1977).

3.2.1. Nearest neighbor search using k-d tree:

The nearest neighbor search (NN) algorithm aims to find the point in the tree that is nearest to a given input point. This search can be done efficiently by using tree properties to quickly eliminate large portions of the search space. Finding the nearest point is an $O(log\ N)$ operation in the case of randomly distributed points.

Analyses of binary search trees has found that the worst case for search time in an k-dimensional KD tree containing N nodes is given by (Lee & Wong, 1977)

$$t_{worst} = O(k.N^{1-\left(\frac{1}{k}\right)}) \tag{3.8}$$

which makes this approach significantly faster than the brute force method.

In very high dimensional spaces, the curse of dimensionality causes the algorithm to need to visit many more branches than in lower dimensional spaces. In particular, when the number of points is only slightly higher than the number of dimensions, the algorithm is only slightly better than a linear search of all of the points. As a rule of thumb, if the dimensionality (of embedding) is k, the number of points in the data, N, should be $N >> 2^k$. In our case $N = 2048$ which implies $N >> (2^k = 2^6 = 64)$ holds true.

3.3. Measures to Detect Information Flow in Coupled Systems

The Transfer Entropy values contain information about which system is the driver and which system is driven. Theoretically, smaller values of $TE_{Y \to X}$ (in a given direction) imply that the amount of information about the next state of X considering the current state of X and Y is small compared to considering only the current state of X.

As we move from bivariate time series to multivariate time series we are dealing with several drivers and several response systems (driven systems). To address this situation, we develop bivariate measures that quantify the involved variables' relative strength of driving in pairs. We propose four such measures: Outflow (TEO), Inflow (TEI), TE Net Outflow (TEN), and TE Average Outflow (ATE). It is important to analyze each of these measures and has meaning only

when the system under consideration has several subsystems with varying coupling strengths and directions.

Consider a large complex system with k coupled sub-systems $\{x_i\}_{i=1}^{k}$. We have $\binom{k}{2}$ pairs $(x_{i,n}, x_{j,n})$ where TE is estimated from data points $x_{i,n}$, with n running from $1, \dots, N$ for all combinations of i and j. $TE_{i\to j}$ then denotes the transfer entropy outflow from the i^{th} subsystem to the j^{th} subsystem. We use this terminology for all measures discussed below.

3.2.1 TE Outflow (TEO)

Transfer Entropy is first estimated for all $\{x_{i,n}\}_{i=1}^{k}$ in the 'outward' direction. TEO is defined as

$$TEO_i = \frac{1}{k-1}\sum_{\substack{j=1 \\ j\neq i}}^{k} TE_{i\to j} \tag{3.9}$$

In systems where couplings are sparse and localized, subsystems may have stronger connection with just a few other subsystems. Here the connection with the maximum values may be of interest. Therefore, we modify the above equation as follows

$$TEO'_i = \max_{\forall\, j, j\neq i} TE_{i\to j} \tag{3.10}$$

3.2.2 TE Inflow (TEI)

Transfer Entropy is estimated for all $\{x_{i,n}\}_{i=1}^{k}$ in the 'inward' direction. TEI is defined as

$$TEI_i = \frac{1}{k-1}\sum_{\substack{j=1 \\ j\neq i}}^{k} TE_{j\to i} \tag{3.11}$$

Similarly, using the maximum inflow metric, we have

$$TEI'_i = \max_{\forall\, j, j\neq i} TE_{j\to i} \tag{3.12}$$

3.3.3 TE Net Outflow (TEN)

Transfer Entropy is estimated for all $\{x_{i,n}\}_{i=1}^{k}$ in both directions. TEN is defined as

$$TEN_i = \frac{1}{k-1}\sum_{\substack{j=1 \\ j\neq i}}^{k} (TE_{i\to j} - TE_{j\to i}) \tag{3.13}$$

The difference $TE_{i\to j} - TE_{j\to i}$ has an expected value of zero for either independent or completely dependent and equally bidirectional dynamics between i and j. Non-zero differences characterize an existing direction of coupling.

For sparse coupling

$$TEN'_i = \max_{\forall\, j, j\neq i} (TE_{i\to j} - TE_{j\to i}) \tag{3.14}$$

3.3.4 Average TE Outflow (ATE)

Here Transfer Entropy is estimated for all $\{x_{i,n}\}_{i=1}^{k}$ in both directions. Then ATE is defined as

$$ATE_i = \frac{1}{k-1}\sum_{\substack{j=1 \\ j\neq i}}^{k} \frac{TE_{i\to j} + TE_{j\to i}}{2} \tag{3.15}$$

In cases where the overall strength rather than the direction of coupling is of importance, ATE is preferred. ATE values are distributed around zero for

realizations of independent dynamics between I and j. Increasing coupling strengths are generally reflected in increasing values of ATE.

Similarly as before, for maximum strength of coupling we define

$$ATE_i = \max_{\forall\, j, j \neq i} \frac{TE_{i \to j} + TE_{j \to i}}{2} \tag{3.16}$$

Chapter 4

APPLICATION OF TRANSFER ENTROPY TO COUPLED DYNAMICAL SYSTEMS

4.1. Discrete Models: System of Coupled Henon maps

Consider two nonlinearly coupled Henon systems given by the equations

$$x_{1,n+1} = 1.4 - \left(\epsilon_1 x_{2,n} x_{1,n} + (1-\epsilon_1) x_{1,n}^2\right) + 0.3 x_{1,n-1} \tag{4.1}$$

$$x_{2,n+1} = 1.4 - \left(\epsilon_2 x_{1,n} x_{2,n} + (1-\epsilon_2) x_{2,n}^2\right) + 0.3 x_{2,n-1} \tag{4.2}$$

where ϵ_1, $\epsilon_2 \in [0,1]$ are the coupling coefficients between the two maps.

The data $x_1(n)$ generated from Equation 4.1 will be referred to as H_1 and $x_2(n)$ from Equation 4.2 will be referred to as H_2. We estimate $TE_{X\to Y}$ and $TE_{Y\to X}$ using both the Correlation Integral method (TE_{CI}) and the Nearest Neighbor approach (TE_{NN}). For both methods of TE estimation, the embedding dimensions k and l in Equation 2.15 are chosen to be 2 and 1 respectively, and $\tau = 1$.

Robustness of TE estimation to noise

A total of 204,800 data points were generated from the above model. The coupling was kept constant at $\epsilon_1 = 0$, $\epsilon_2 = 0.6$ which established unidirectional coupling from $H_1 \to H_2$. White Gaussian noise was added to the time series from H_1 and H_2 for different SNR (signal-to-noise-ratio) values, TE was estimated for 100 segments of 2,048 points each. The mean and standard deviation of TE is shown in Figure 4.1.

Both methods for estimation of TE showed consistent behavior for large SNR values, being able to distinguish the driver and driven maps. TE_{CI} showed a drop in TE values for less than 15 dB SNR, while TE_{NN} showed more robustness to noise even around 1 dB SNR although its standard deviation increased.

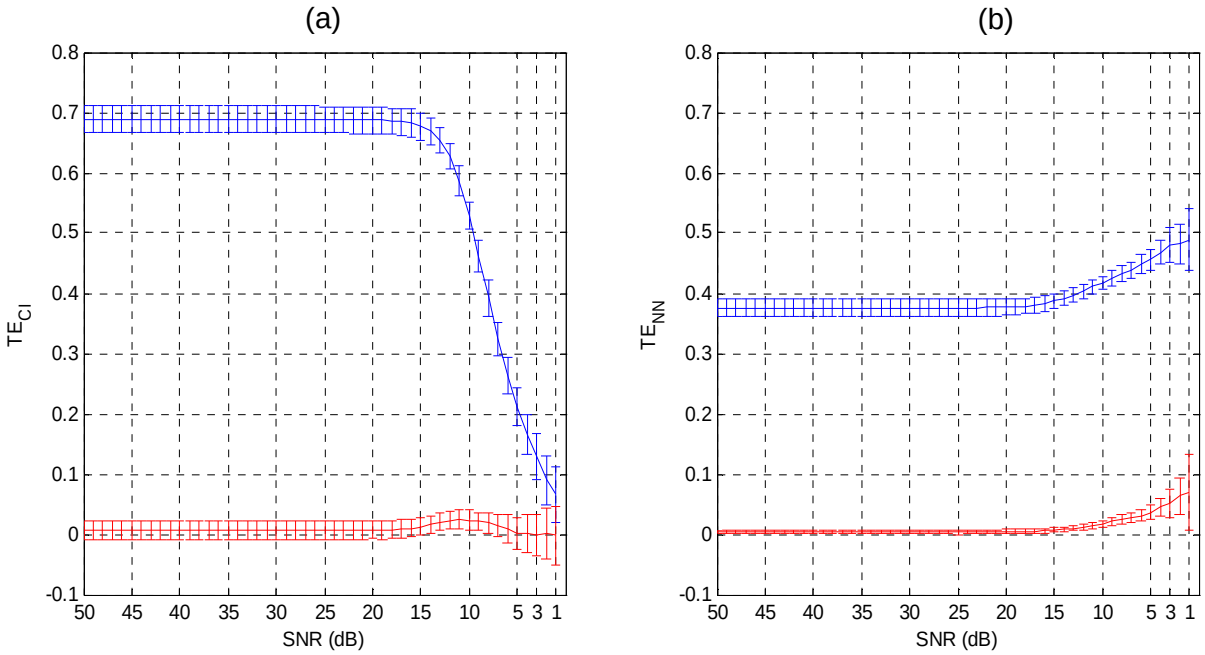

Figure 4.1. (a) TE_{CI} and (b) TE_{NN} with addition of observational Gaussian noise in a system of two coupled Henon maps. TE_{NN} shows more robustness to noise compared to TE_{CI}. Blue line is TE ($H_1 \rightarrow H_2$) and red line is TE ($H_2 \rightarrow H_1$)

System of many Coupled Henon maps

A system of many coupled Henon maps is described in Figure 4.2. We will use the measures defined in Equations 3.11 through 3.18 to analyze the flow of information in the system and determine the component (individual Henon map) which exhibits largest outflow, largest coupling and the dominant characteristics with respect to information flow. All the Henon time series are generated by Equations 4.1 and 4.2 with the coupling specified in Figure 4.2. The embedding dimension and lag used for TE estimation is the same as in the previous section. All notational conventions are the same as before unless otherwise specified.

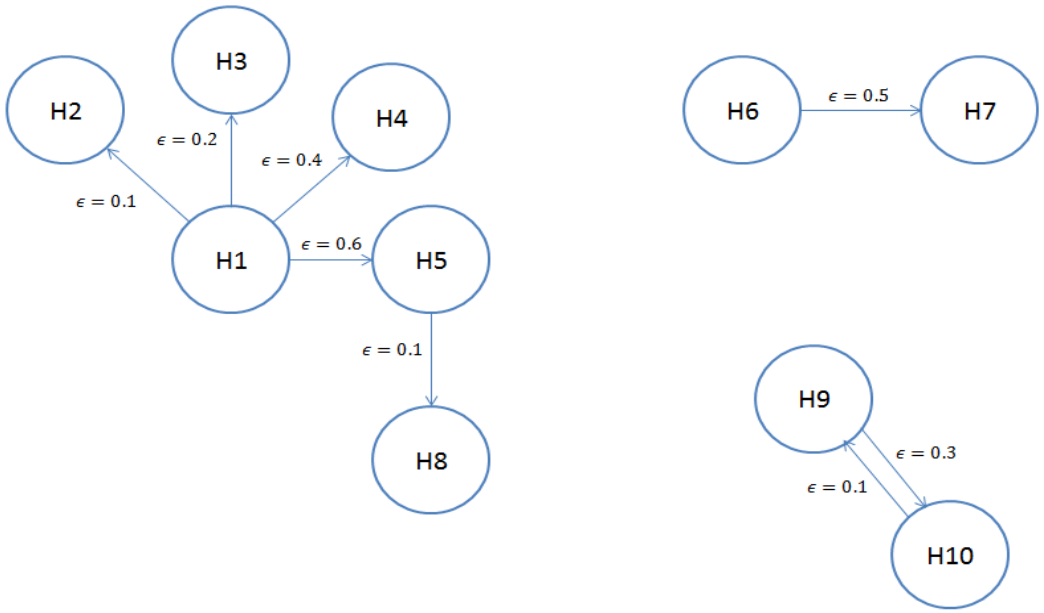

Figure 4.2. Network of Henon maps coupled with different coupling coefficients as specified by the coupling values near the arrows between maps. Arrows show the direction of coupling.

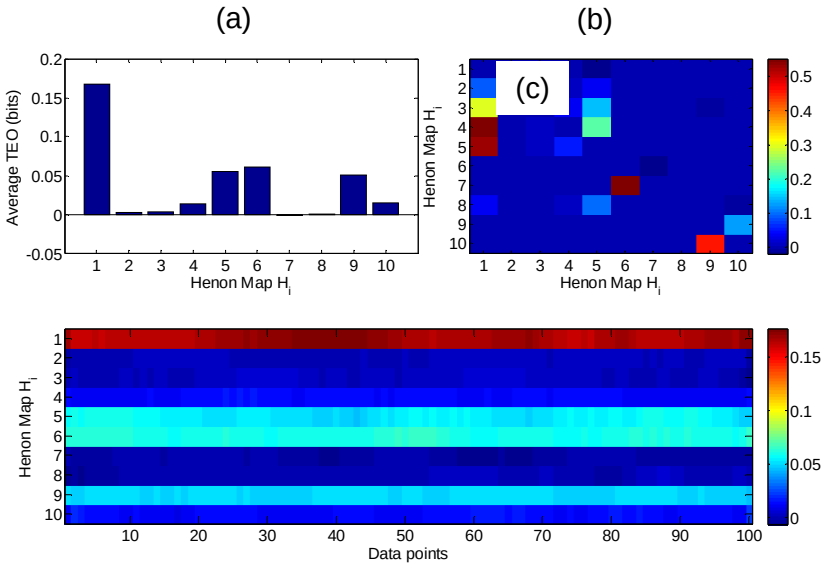

Figure 4.3. TEO for the network system of Henon maps: (a) The average TEO over the entire data, (b) the outflow between pairs of maps in a grid, and (c) Outflow from all Henon maps over time.

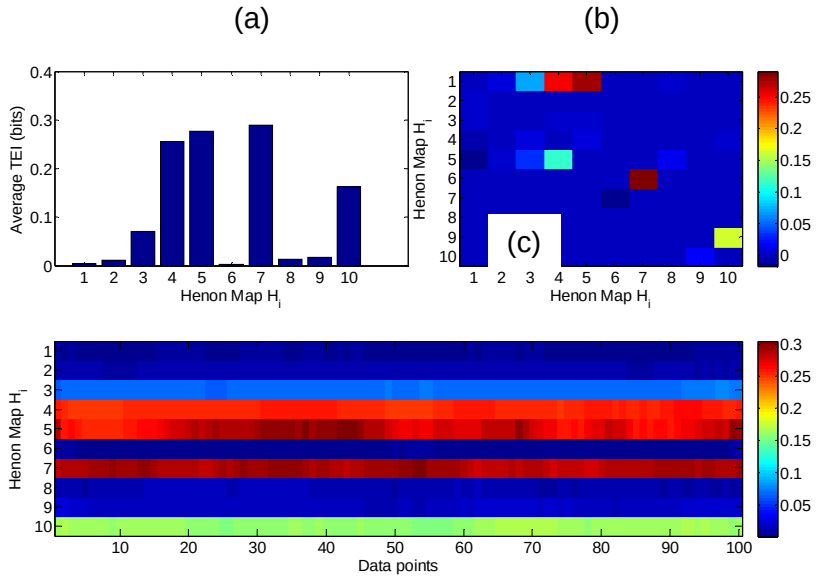

Figure 4.4. TEI for the network system of Henon maps: (a) The average TEI over the entire data, (b) the inflow between pairs of maps in a grid, and (c) Inflow of all Henon maps over time.

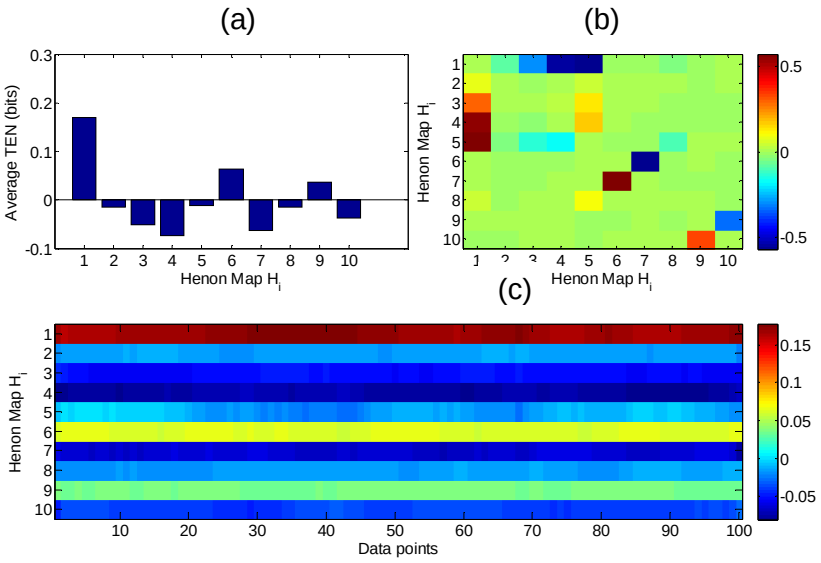

Figure 4.5. TEN for the network system of Henon maps: (a) The average TEN for the entire data, (b) the Net outflow between pairs of maps in a grid, and (c) Net Outflow of all Henon maps over time.

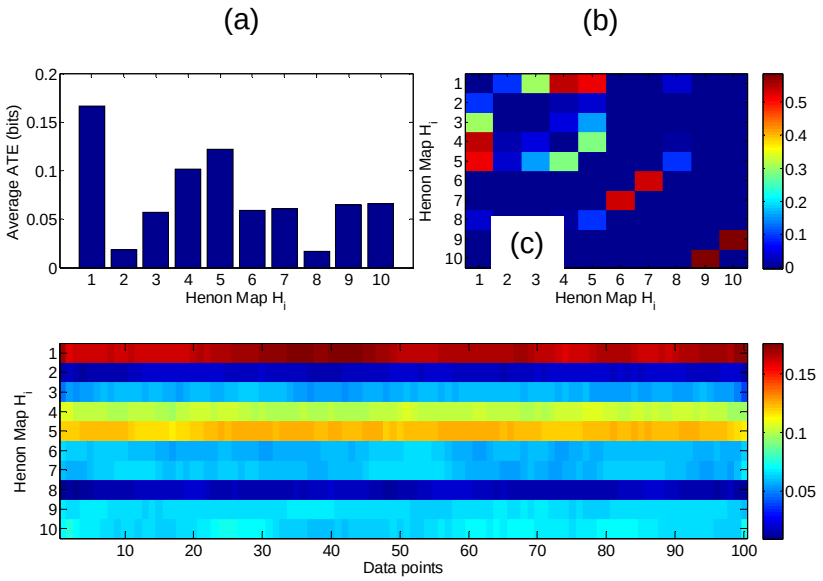

Figure 4.6. ATE for the network system of Henon maps: (a) The average ATE for the entire data, (b) the strength of coupling between pairs of maps, and (c) Average TE of all Henon maps over time.

Discussion

From Figure 4.2 it is clear that H_1 has the highest outflow. This is indeed the case since it has unidirectional couping with H_{2-4}. The H_6 has the second highest outflow due to high coupling strength with H_7 . All the rest of the maps are driven and hence have positive inflow of information. H_8 is only weakly driven by H_5. The H_9 and H_{10} have bidirectional coupling with each other which shows as small values for TEN.

We evaluate our results in the following section in light of the above discussion.

Description of plots

For each of the 4 methods (TEO, TEI, TEN and ATE) we have one Figure with 3 descriptive panels sub labeled (a), (b) and (c). Panel (a) is the plot of the average value for each method over time (or for all data points). This aids in understanding which Henon map H_i has the highest value of a given measure averaged to all other maps. No assumption about the nature of coupling is made, which makes it more suitable for time series from an unknown system. Panel (b) shows pairwise information flow for each method from H_i to H_j $\forall\, i, j$. The color corresponds to the strength of interaction. The value is the time average over all data points. In panel (c) we show the same information as in (a) except that the evolution of the information flow can be observed over time. This proves useful to observe change in the dynamics of information flow over time in systems that coupling changes with time (like in EEG).

Results

In Figure 4.3(a) we observe that H_1 has the highest TEO values of TEO with H_5 and H_6 following it. This is in accordance with the model structure and specified couplings. In Figure 4.3(b), the relevant pairwise information and outflow from H_1 to H_{2-5} can be seen as increasing plot color intensity due to the increase in coupling strength. Figure 4.3(c) shows the same information over time.

Figure 4.4(a) shows the inverse relationship of TEI compared to TEO. H_2, H_3, H_4, H_5 show increasing values of TEI due to increasing coupling strength of the response system. Similar observations are made for plots (b) and (c).

In Figure 4.5(a) it is interesting to observe that only H_1, H_6 and H_9 show positive TEN. This is because only they have Net positive outflow. Although H_5 is

driving H_8, H_5 is driven more strongly by H_1 and hence it has a negative net outflow. Figure 4(b) and (c) show plots supporting the above arguments.

Finally, Figure 4.6 shows that sites with strong coupling in either direction show higher values for ATE.

The above results validate the point that each of the defined four measures in terms of TE highlights unique characteristics in a complex network of coupled systems. Depending on the nature of interactions one is seeking for, the right measure can be utilized. In Chapter 5, we will apply these insights to the EEG, where the nature of interaction and strength of interaction are unknown and changing over time.

4.2. Continuous Models: Systems of Coupled Rossler oscillators

A coupled Rossler system with N Rossler oscillators in the chaotic regime can be written as

$$\dot{x}_i = -\omega_i y_i - z_i \psi_i(\epsilon, x_i, x_j) \tag{4.3}$$

$$\dot{y}_i = -x_i + \alpha_i y_i \tag{4.4}$$

$$\dot{z}_i = \beta_i + z_i(x_i - \gamma_i) \tag{4.5}$$

where $\alpha_i = 0.15$, $\beta_i = 0.2, \gamma_i = 10$ are the parameters for $i = 1 \ldots N$. For our application we use diffusive (linear) coupling, which means $\psi_i(\epsilon, x_i, x_j) = \epsilon(x_j - x_i)$, and $N = 3$.

The coupling is described in Figure 4.7.

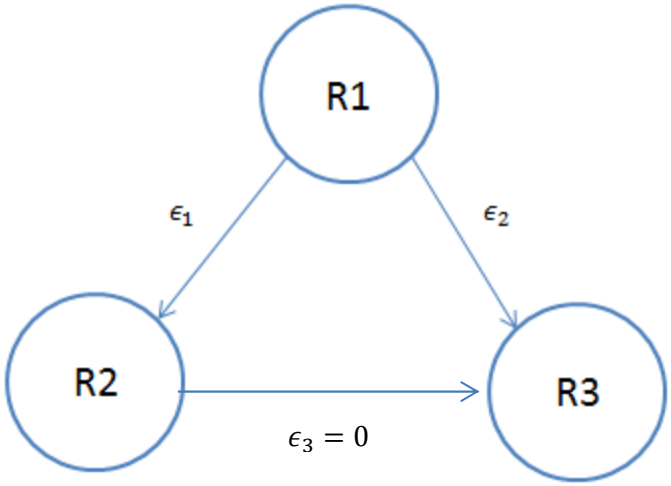

Figure 4.7. A coupled system with 3 Rossler oscillators (R1, R2 and R3) and their coupling $\epsilon_1 and\ \epsilon_2$.

We will once again use the measures defined in Equations 3.11 through 3.18 to analyze the flow of information in the system and determine the component (R1, R2 or R3) that exhibits largest outflow, largest coupling and the dominant characteristics with respect to information flow. All Rossler time series R1(t), R2(t) and R3(t) are generated by Equations 4.3 to 4.5 with varied coupling. 102,400 data points were generated per coupling value. The embedding dimension $m = 3$ and lag $\tau = 4$ was determined by using methods from section 2.3 for TE estimation. TE is estimated for non-overlapping points of window size = 2048 points. $k = 3$ and $l = 1$ are chosen as the embedding dimension of the Rossler.

Effect of TE on variation of coupling

The effect of variation in coupling strength is shown in Figure 4.8. It can be seen that TE between two Rossler oscillators has higher values when the coupling

strength is higher. The coupling is changed every 50 TE points (or 102,400 points in the original time series.). The coupling strengths are shown in Figure 4.8.

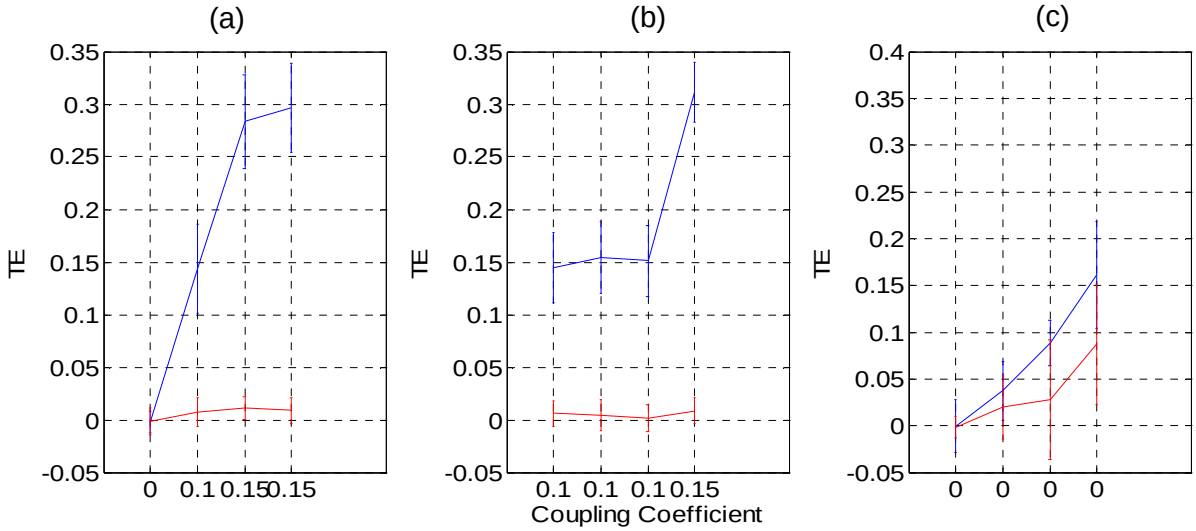

Figure 4.8. (a) Variation of $TE_{R1\rightarrow R2}$ with respect to variation in coupling coefficient. (b) Same for $E_{R1\rightarrow R3}$. (c) Same for $TE_{R2\rightarrow R3}$.

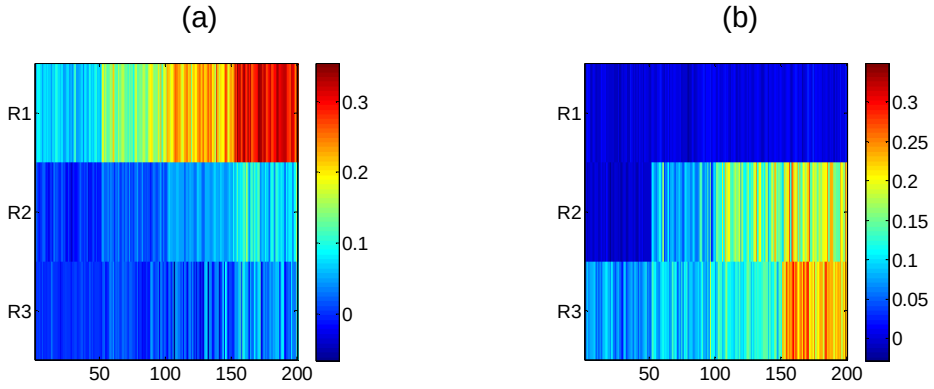

Figure 4.9 (a) $O_i \; \forall \; i = R_1, R_2, R_3$. (b) $TEI_i \; \forall \; i = R_1, R_2, R_3$

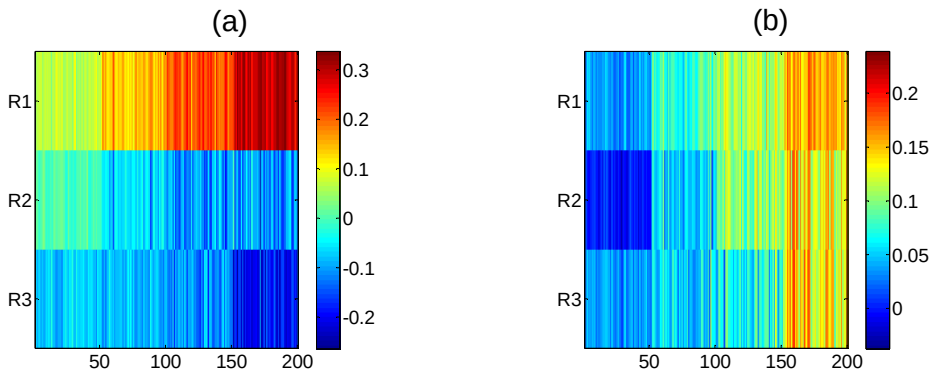

Figure 4.10 (a) $N_i \; \forall \; i = R_1, R_2, R_3$. (b) $ATE_i \; \forall \; i = R_1, R_2, R_3$

Discussion

From Figure 4.9(a) we can see that TEO_{R1} is always higher than TEO_{R2} and TEO_{R3} due to the nature of the existing coupling in the system. TEO_{R2} and TEO_{R3} are roughly zero since there is no effective outflow due to the existing unidirectional coupling inwards.

Figure 4.9(b) shows TEI_{R1} to be close to zero throughout since there is no inflow to R1. R2, which is not driven for the first 50 points, shows zero TEI_{R2} and then increases once the coupling between $R1 \rightarrow R2$ becomes non zero. The color intensity which is an indication of the amount of inward information flow increases as the coupling increases.

Figure 4.9(c) shows better results than the above two for R1 since all bias, if any, is removed due to the way TEN_i is calculated. Finally Figure 4.9(d) shows the average outflow and we can observe that both $ATEN_{R2}$ and $ATEN_{R3}$ have higher values when the coupling of R2 and R3 with R1 increases (by the end of the record). We also observe that TEN_{R1} is also high in this period.

Chapter 5

APPLICATION OF TRANSFER ENTROPY TO DYNAMICS OF EPILEPTIC BRAIN

5.1. Introduction

Epilepsy is considered a “sacred” or “divine” disease and is among the most common disorders of the nervous system, second only to stroke, and affects 1-2% of the world’s population (Engel, Pedley, & Aicardi, 2008). Estimates of incidence rates (number of new cases per year) range from 24 to 53 per 100,000. The high incidence of epilepsy stems from the fact that it occurs as a result of a large number of causes, including genetic abnormalities, developmental anomalies, febrile convulsions, as well as brain insults such as craniofacial trauma, central nervous system infections, hypoxia, ischemia, and tumors.

The hallmark of epilepsy is recurrent seizures. If seizures cannot be controlled, the patient experiences major limitations in family, social, educational, and vocational activities. These limitations have profound effects on the patient’s quality of life, as well as on his or her family (Goldstein & Harden, 2000). The seizures are due to sudden development of synchronous neuronal firing in the cerebrum and are recorded by electrodes on (scalp) or inside (intracranial) the brain. Seizures may begin locally in portions of the cerebral hemispheres (partial / focal seizures with a single or multiple foci) or simultaneously in both cerebral hemispheres (generalized seizures). After a seizure’s onset, partial seizures may remain localized and cause relatively mild cognitive, psychic, sensory, motor, or autonomic symptoms, or may spread (secondarily generalized) to cause altered

consciousness, complex automatic behaviors, or bilateral tonic-clonic (convulsive) movements.

Because seizures typically occur without a warning to the patient, localization of the epileptogenic focus requires a long stay (days) of the patient in a well-controlled, long-term EEG recording clinical environment, the epilepsy monitoring unit (EMU), while the patient's anti-epileptic medication is progressively tapered. The goal is for the patient to have several (usually 3 to 4) of his/her typical seizures in order for the physicians to localize the focus with confidence. Continuous video of the patient is also recorded for the physicians to correlate the observed clinical symptoms in the video with the findings from the EEG (Gotman, Gloor, & Ives, 1985). Focus localization at EMUs through visual inspection of the recorded EEG has variable rates of success. For example, up to 20-50% of pediatric EMU evaluations do not capture any epileptic events (Asano et al., 2005). In a mixed group of children and adults who attained post-operative seizure-freedom, the EEG had correctly localized the focus only 70% of the time, and even less so for extra-temporal epilepsies, for which the EEG also had falsely localized the focus up to 25% of the time (Manford, Hart, Sander, & Shorvon, 1992).

Classifying epilepsy as focal or generalized guides selection of anticonvulsants, aids classification into an epilepsy syndrome, and determines whether neuro-imaging is needed for further localization. Typically, only patients rendered focal by the EEG proceed for neuroimaging studies. Multiple imaging modalities can be used during a presurgical evaluation: magnetic resonance imaging (MRI), positron emission tomography (PET), Subtraction Ictal Single-photon-emission-computed-tomography (SPECT) Co-registered with MRI

(SISCOM), and magnetoencephalography (MEG). However, these modalities have serious limitations too. For newly diagnosed focal epilepsy from phase I, 12-13% of cases are symptomatic (cerebral lesion visible with neuro-imaging) and 18-29% are cryptogenic (cerebral lesion not visible with neuro-imaging) (Loiseau et al., 1990). While the presence of a surgically remediable lesion on MRI improves post-surgical seizure freedom to 70-90%, a clinically relevant lesion is found only 15-20% of the time.

The mainstay of treatment of epilepsy today is pharmacological. Nonetheless, 30-40% of patients with epilepsy have seizures that are refractory to medical therapy (medically refractory or clinically intractable) (Kwan & Brodie, 2000; Schiller & Najjar, 2008). For these patients, surgical treatment may then be the only option for seizure control. However, surgical treatment can be effective in carefully selected cases, usually 8-10% of the total epileptic patients (Engel Jr, Van Ness, Rasmussen, & Ojemann, 1993), for whom the focus location can be rendered with high confidence and ablation of focus is not expected to sever nearby critical brain centers. Good responses (Engel Class I) to surgery occur in approximately 70-90% of adult patients with complex partial seizures due to mesial temporal sclerosis. However, the response rate drops off markedly (50-60%) in patients with epileptogenic lesions of the neocortex (most commonly in frontal or temporal lobes). Patients diagnosed with more than one epileptogenic focus, or those with generalized seizures, usually do not experience complete seizure control with current surgical therapy. This is a good example of the role an accurate diagnosis of the location and extent of the epileptogenic focus plays in the treatment of epilepsy.

It is widely believed that seizures arise from the epileptogenic focus (also called epileptogenic zone to emphasize the network dimension of it) because of damage in key brain structures and/or networks. For example, damage to hippocampal circuitry causes seizures of mesial temporal lobe origin. The characteristic circuit abnormalities include drop out of neurons, loss of neurotransmitter receptors, simplification of the dendritic tree (reduced synaptic input), sprouting of dentate granule cell axons (increase of the number of excitatory-excitatory feedback connections), and increase in glial cell elements (sclerosis) (Koblar, Black, & Schapel, 1992). Physiological studies in epileptogenic hippocampi have demonstrated loss of neuronal inhibition. It is generally believed that impairment of the balance of inhibition and excitation at the neuronal network level is one critical factor for epileptogenesis (Dudek & Spitz, 1997). Clinical research in controlling of seizures via electromagnetic (e.g., deep brain stimulation – DBS) or in-situ pharmacological stimulation has started and is expected to flourish in the near future within the new field of neuromodulation (Lopes da Silva & Pijn, 1995). A basic question that needs to be answered is where to stimulate, especially with respect to the focal zone. This is another good example where localization of the focus and its extent is a problem that needs to be solved accurately for an epilepsy treatment to be effective.

Our research may shed light on epileptogenesis by providing, tools for EEG monitoring of epileptogenic foci in patients with the disorder under development.

5.2. Long Term EEG Monitoring

In this thesis, the methods developed in the previous chapters are applied to EEG data from two patients with epilepsy. The patients underwent presurgical

evaluation and long-term intracranial EEG recordings, and subsequent successful (Engel's class I) surgery with removal of the clinically identified epileptogenic focus. These stored pre-surgical, long-term, continuous EEG recordings of several days in duration, were used to test our methodologies. Informed consent for participation in this study was obtained from all patients. The recording procedures and the data recorded and analyzed are detailed below.

The two patients underwent a stereotactic placement of:

1.) Bilateral depth electrodes the hippocampi (RTD1 anterior, RTD6 posterior, in the right hippocampus, with RTD1 adjacent to right amygdala; LTD1 anterior, LTD6 posterior in the left hippocampus with the LTD1 adjacent to the left amygdala).
2.) Two subdural strip electrodes were placed bilaterally over the orbitofrontal lobes (LOF1 to LOF4 in the left and ROF1 to ROF4 in the right lobe, with LOF1, ROF1 being most mesial and LOF4, ROF4 most lateral).
3.) Two subdural strip electrodes were placed bilaterally over the temporal lobes (LST1 to LST4 in the left and RST1 to RST4 in the right, with LST1, RST1 being more mesial and LST4 and RST4 being more lateral).

Video/EEG monitoring was performed using the Nicolet BMSI 4000 EEG machine. EEG signals were recorded using an average common reference with band pass filter settings of 0.1 Hz – 70 Hz. The data were sampled at 200 Hz.

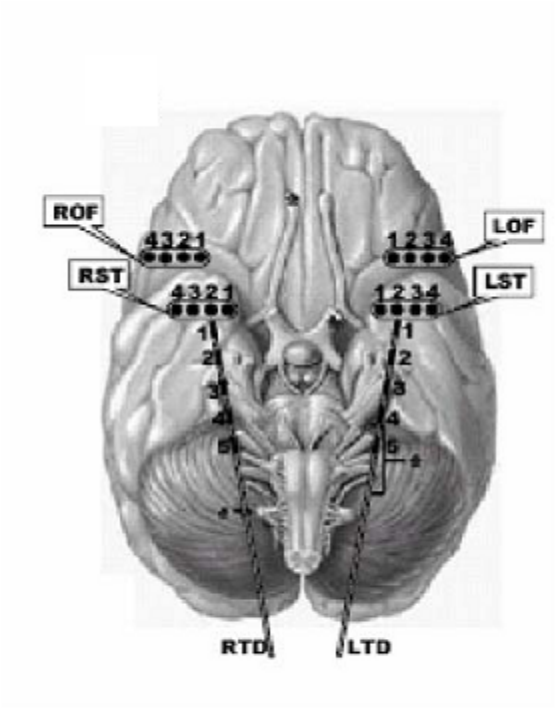

Figure 5.1. Schematic diagram of an horizontal section of the brain showing the depth and subdural electrode placement.

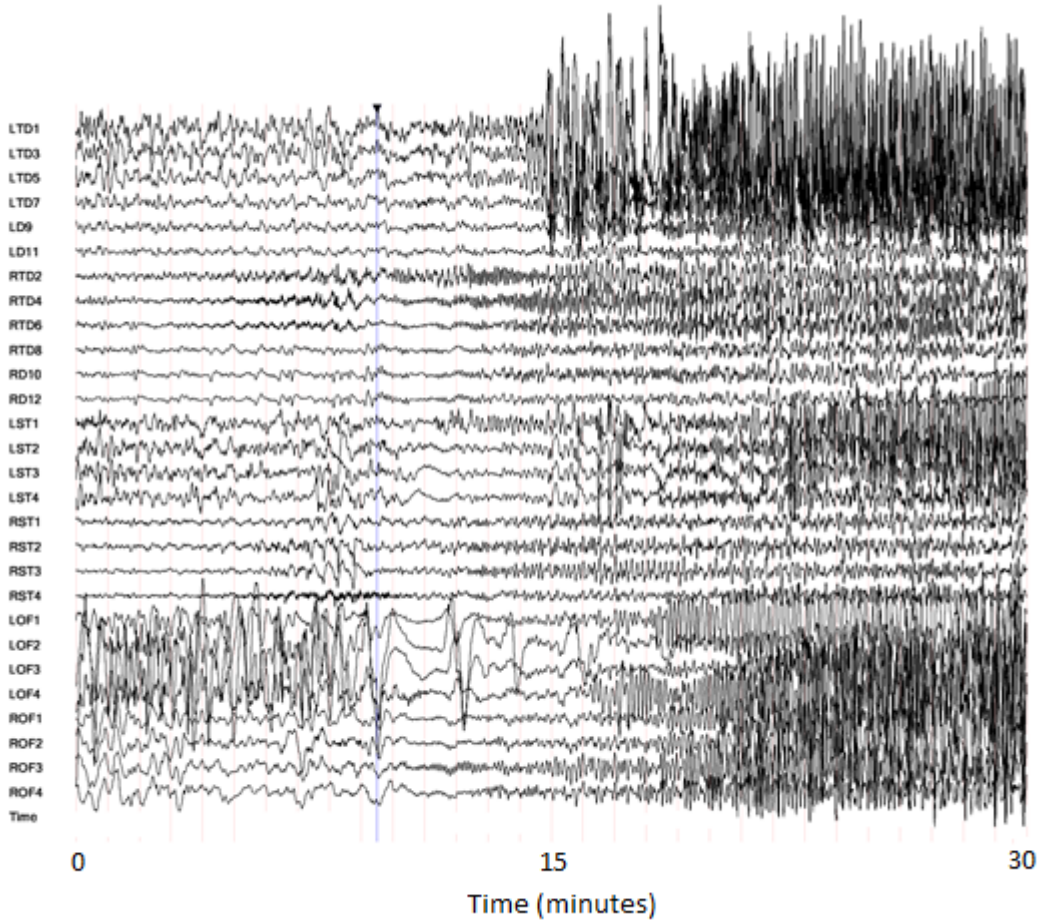

Figure 5.2. EEG at the beginning of a seizure in patient 1. Seizures are bursts of sudden, relatively brief disturbances of brain's function caused by hypersynchronous abnormal paroxysmal cerebral electrical activity. Seizure starts at RTD (hippocampus focus) and then spreads to other channels (brain sites).

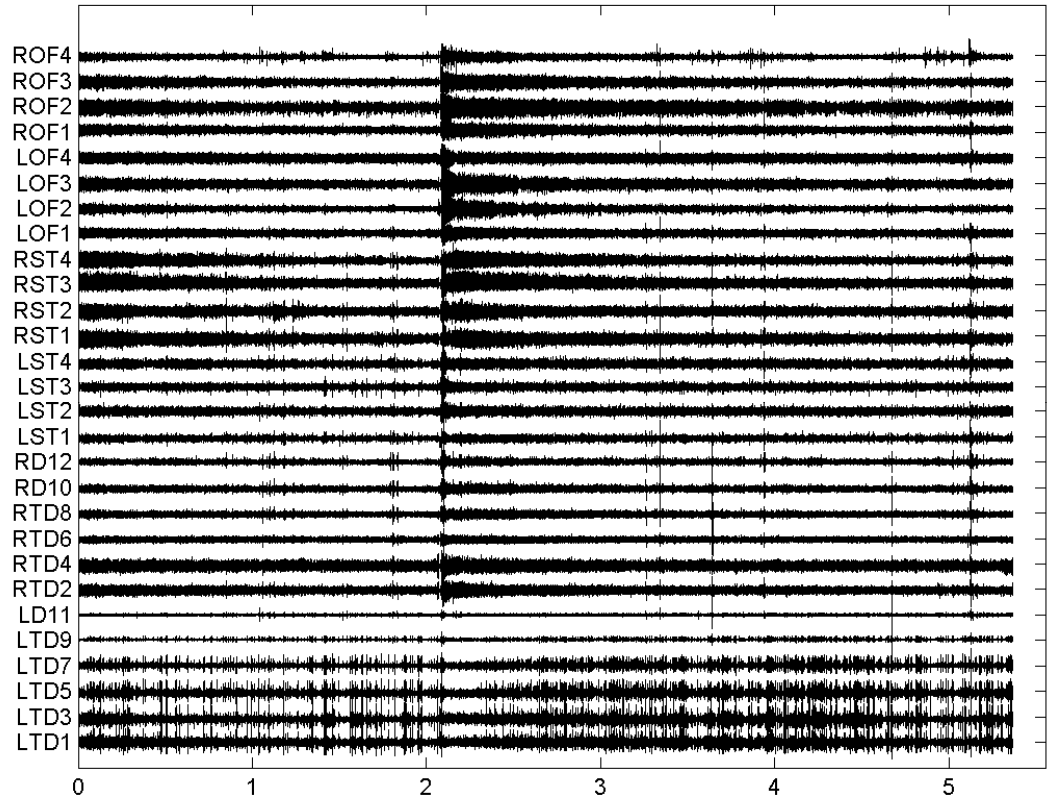

Figure 5.3. EEG from one full tape of recording around a seizure spanning 5 hours 22 minutes.

5.3. Estimation of Transfer Entropy, TEO, TEI, TEN and ATE for EEG

In chapter 4 we discussed the application of Transfer Entropy (TE) to coupled chaotic attractors. In this chapter, we apply the methods developed to EEG data from patients with epilepsy. The choice parameters k and l (order of the Markov process for the driven and driving system) are important to approximately capture the information transfer in the brain taking into account the changes in the underlying dynamics of the system. We previously observed that the radius r in the estimation of TE affects the probability distribution and hence the estimate for

TE. Extension of these concepts to real world data like EEG is simple though not trivial. We maintain l-Markov order of the driving system to be 1, as suggested in (Schreiber, 2000), to investigate mostly direct (very fast) interactions of the driving system with the driven ones. The k-Markov order was chosen by methods detailed for embedding dimension in Chapter 3 (EEG segments of 2048 points, that is, 10.24 sec in duration). The radius r for the calculation of the involved transition probabilities is chosen as the value where we observe the first linear region of the $lnC(r)/\ln(r)$ curve per EEG segment. This value was found to be around 0.7 of the standard deviation of the recorded EEG data.

TE is estimated from successive, non-overlapping EEG segments of 10.24 seconds in duration (2048 points at 200 Hz sampling rate). The EEG signals were recorded from a total of 28 electrodes. TE values are estimated for both direction ($TE_{Y\to X}\ and\ TE_{X\to Y}$) and for every pair of sites (x, Y).

Iasemidis et al., in (L. D. Iasemidis, Chris Sackellares, Zaveri, & Williams, 1990) (L. Iasemidis & Sackellares, 1991), have shown that a selection of duration of 10.24 sec is adequate for the convergence of the estimates of measures of dynamics from the nonstationary EEG signals in epilepsy.

Proceeding, we estimate Equation 3.11 – 3.18 for all the EEG data from both patients using the optimized TE algorithms discussed in section 5.3. Surrogate analysis was performed (using shuffled data from the driven system to break any existing connectivity in the surrogate data) for bias removal. The analysis of the generated data showed very little bias, of low variance, and did not significantly affect the estimation of TE.

The results for all four measures TEO_i, TEI_i, $TEN_i$and ATE_i are shown in Figure 5.4 during ictal and interictal period.

Description of plots

For each of the 4 methods (TEO, TEI, TEN and ATE) we use the color plots for presentation purposes, which clearly show the values of the measure for each electrode on the average across the rest of the rest of the electrodes over time. In Figure 5.4 (a), it is interesting to observe the changes in value of the measure right after a seizure (e.g., RST3). The vertical axis has the montage with labeled electrodes. The horizontal axis is time. The color bar on the side of the plots gives the scale or reference for color and value of the measure. The red end of the color spectrum denotes higher measure values and the blue end of the spectrum denotes lower values. In Figure 5.4 (a) it is also interesting to observe red values for RTD6 over time. This indicates that RTD6 has higher outflow of information (TEO) compared to other sites which have colors denoting lower intensity.

Observations:

The following observations can be made with regard to the 4 measures for the two patients. The observations are categorized by their applicability to different applications (discussed below in subsequent sections).

Application to Epileptogenic Focus Localization

- The highest outflow over time is observed in RTD 6 (Figure 5.4 (a))
- The highest inflow over time is observed in RTD 4 (Figure 5.4 (b))
- The highest coupling (strength of interaction) is observed in RTD. (Figure 5.5 (b))
- RTD 6 is observed to ‘drive‘ the other sites most of the times. (Figure 5.5 (a), 5.6 (a))

Application to Epileptogenic Focus Lateralization

- LTD, LST, LOF (Left hemisphere) and ROF (Right Frontal) show significantly less activity compared to RTD, RST region. (Figure 5.4, 5.5 (a) and (b)) The epileptogenic zone for these patients was RTD, RST.

Application to Seizure Detection and Understanding of Seizure Dynamics

- Postictal transition shows a significant drop in information flow across all channels (Inflow and Outflow). (Figure 5.4 and 5.5) RST suffers the greatest disruption in information flow in magnitude and duration postictally. (Figure 5.4 and 5.5, 5.6)

Application to Seizure Prediction and Understanding of Seizure Dynamics

- RST shows a steady increase in information flow, until seizure breaks connectivity and resumes progressively increasing postictally. (Figure 5.4 and 5.5, 5.6)

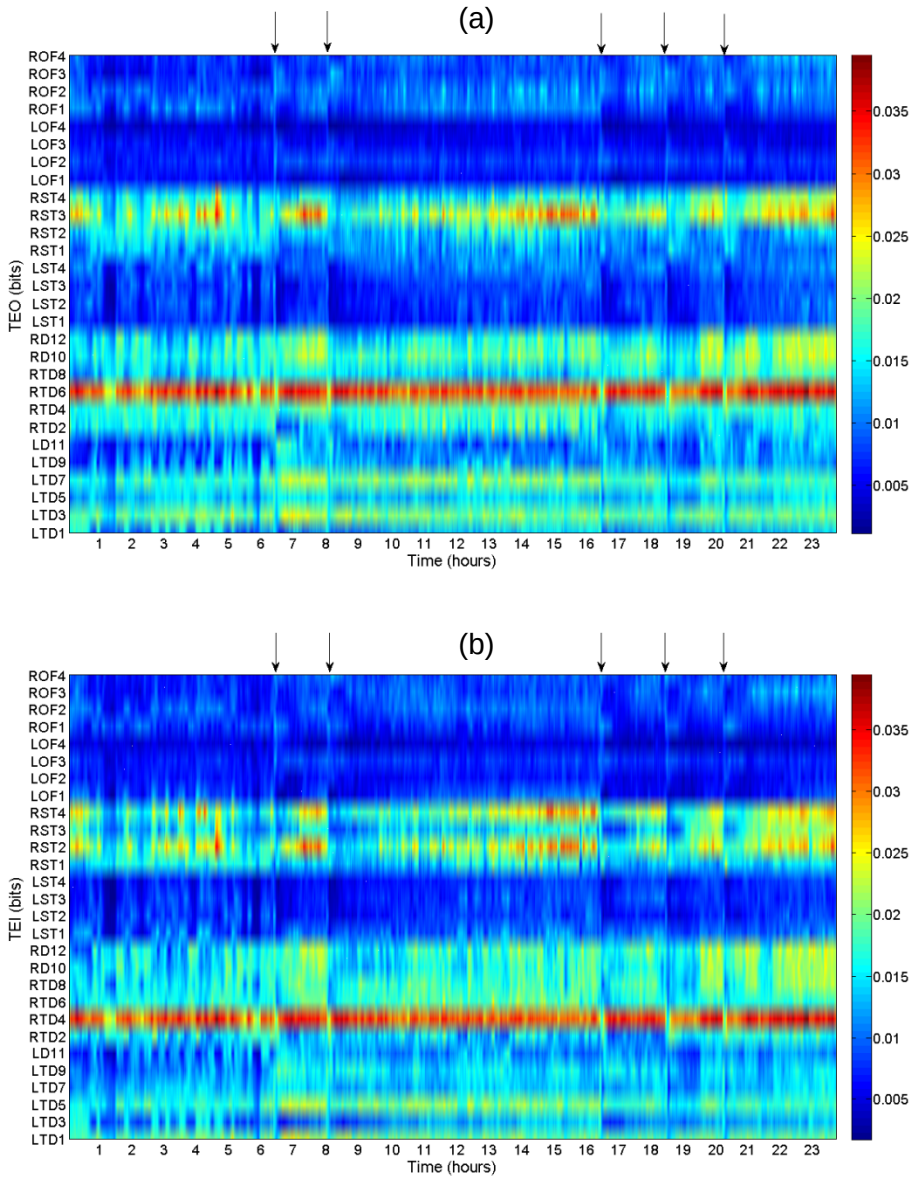

Figure 5.4. Patient 1: (a) $TEO_i \; \forall \; i$ vs. time. (b) Similar plot for I_i . Arrows denote the occurrence of seizures in the analyzed EEG record.

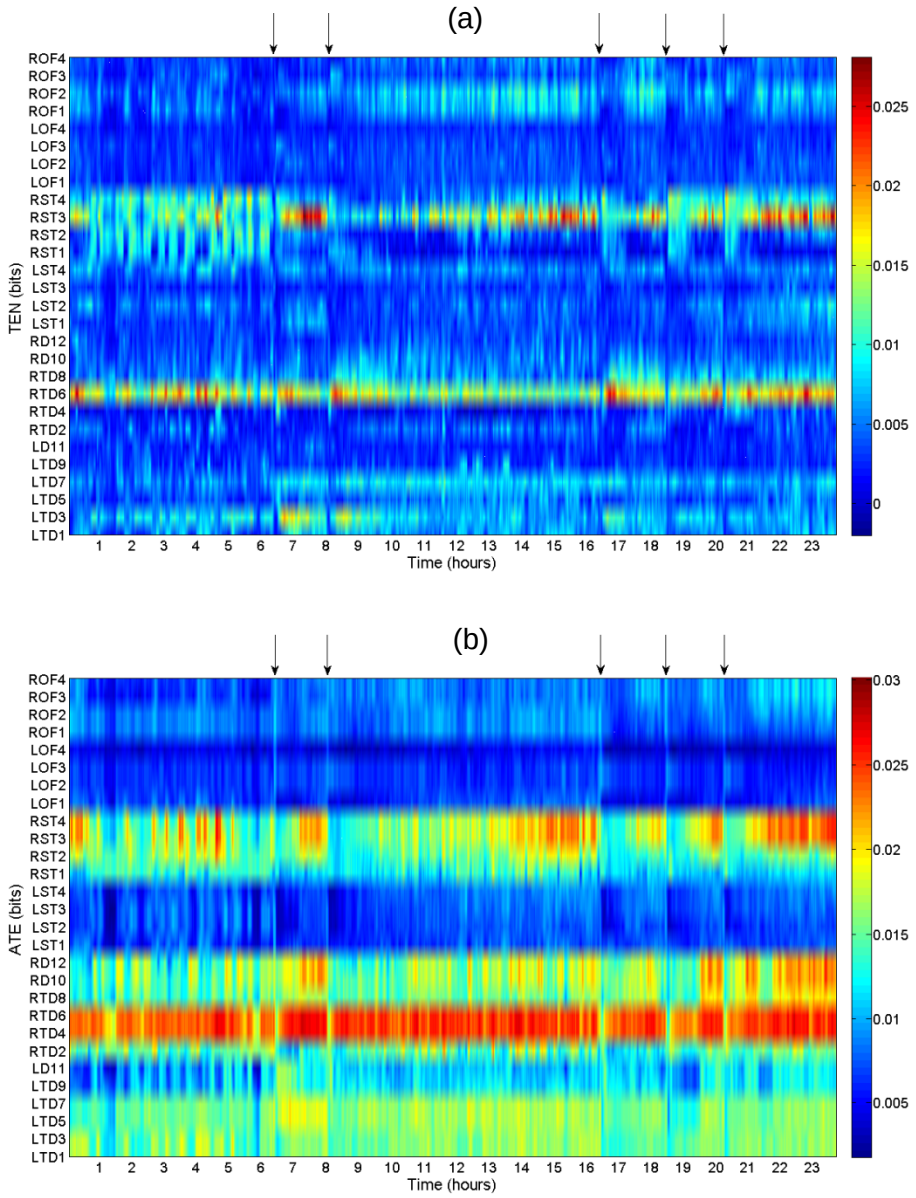

Figure 5.5. Patient 1: (a) $TEN_i \; \forall \; i$ vs. time. (b) Similar plot for ATE_i . Arrows denote occurrence of seizures in the analyzed EEG record.

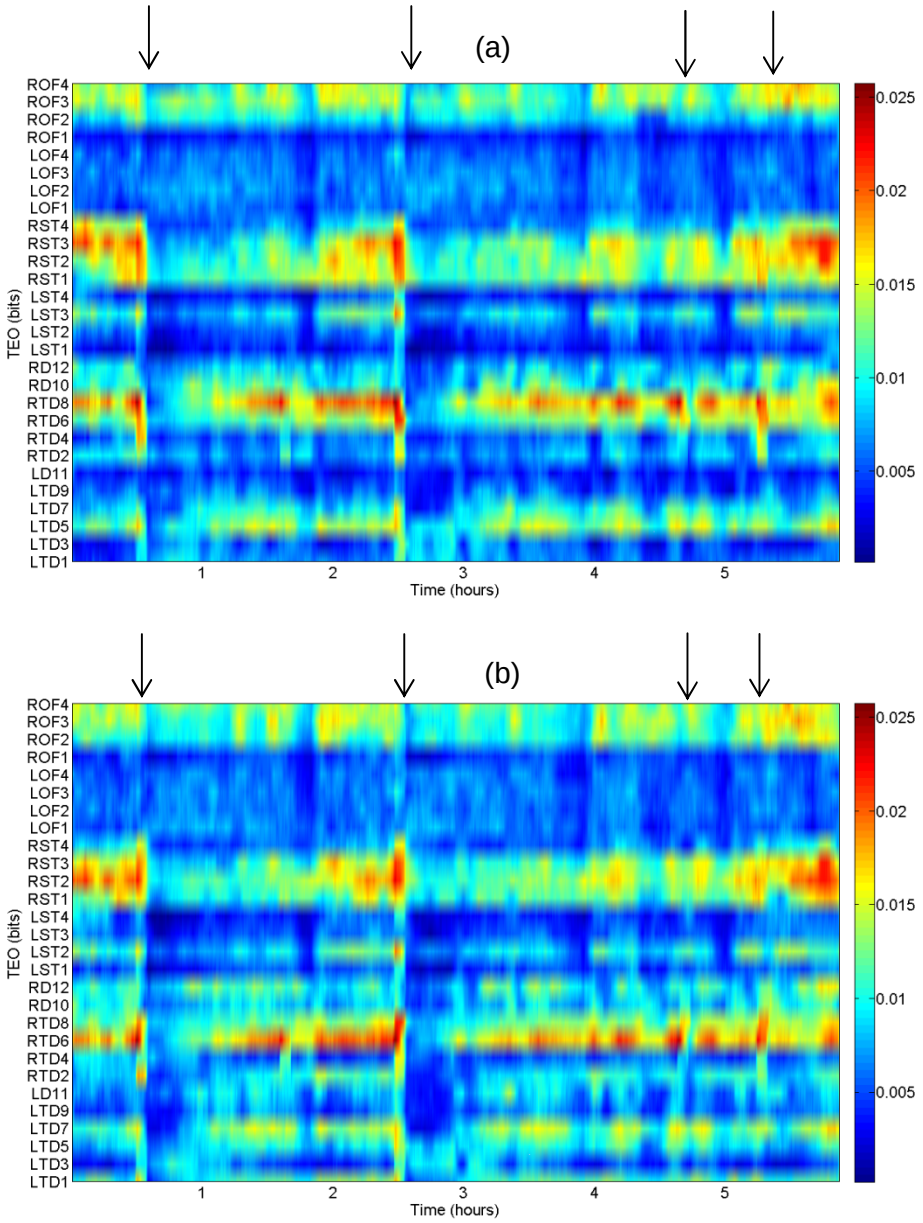

Figure 5.6. Patient 2: (a) $TEO \; \forall \; i$ vs. time. (b) Similar plot for ATI_i . Arrows denote occurrence of seizures in the analyzed EEG record.

5.4. Information Flow in Preictal and Postictal transition

In light of the above plots, and the consistency of the above observations across seizures in the two patients, we postulate that the information flows (TEO_i and ATE_i) at the focal electrodes (RTD) show a significant drop in value postictally.

This denotes a breakage of information flow (breakage of coupling among sites) due to a seizure. This is typically observed in the epileptogenic areas and is in agreement with a past hypothesis of our group about the resetting power of seizures.

In order to test this hypothesis, we performed a test to see if the drop in the mean value of the measures from pre to post seizure is statistically significant compared to transition at a randomly selected point in time interictally. This was evaluated by performing a right-tailed unpaired two-sample t-test for the measures between samples taken five minutes from the immediate preictal period and five minutes from the immediate postictal region. The objective was to observe a significant difference in the means of the two samples. The t-statistic was calculated as

$$T_{pre-post} = \frac{\overline{X_1} - \overline{X_2}}{s_{\overline{X_1}-\overline{X_2}}} \tag{5.1}$$

where

$$s_{\overline{X_1}-\overline{X_2}} = \sqrt{\frac{(s_1^2 + s_2^2)}{n}} \tag{5.2}$$

and s^2 is the unbiased estimator of the variance of the two samples. The $T_{pre-post}$ is calculated for a data sample of $n = 30$ TE points preictally and postictally (which roughly corresponds to 5 minutes pre seizure and 5 minutes post seizure). The seizure durations were taken as 12 points in the TE profiles (roughly 2 minutes) as the gap between the two samples.

A t-statistic distribution was generated for $T_{pre-post}$ using TEO_i or ATE_i $(i \rightarrow RTD)$ values by performing the t-test as mentioned above. For the statistical

evaluation we employed a sliding axis with pre and post windows over the entire duration of the recording. The generated $T_{pre-post}$ distribution was used to check the statistical significance of the difference in mean (or drop in information flow: TEO_i and ATE_i) while transitioning from preictal to postictal periods.

It can be seen from Figure 5.7 that the $T_{pre-post}$ pre- to postictal transitions for TEO_{RTD} and ATE_{RTD} are statistically significant (low p values).

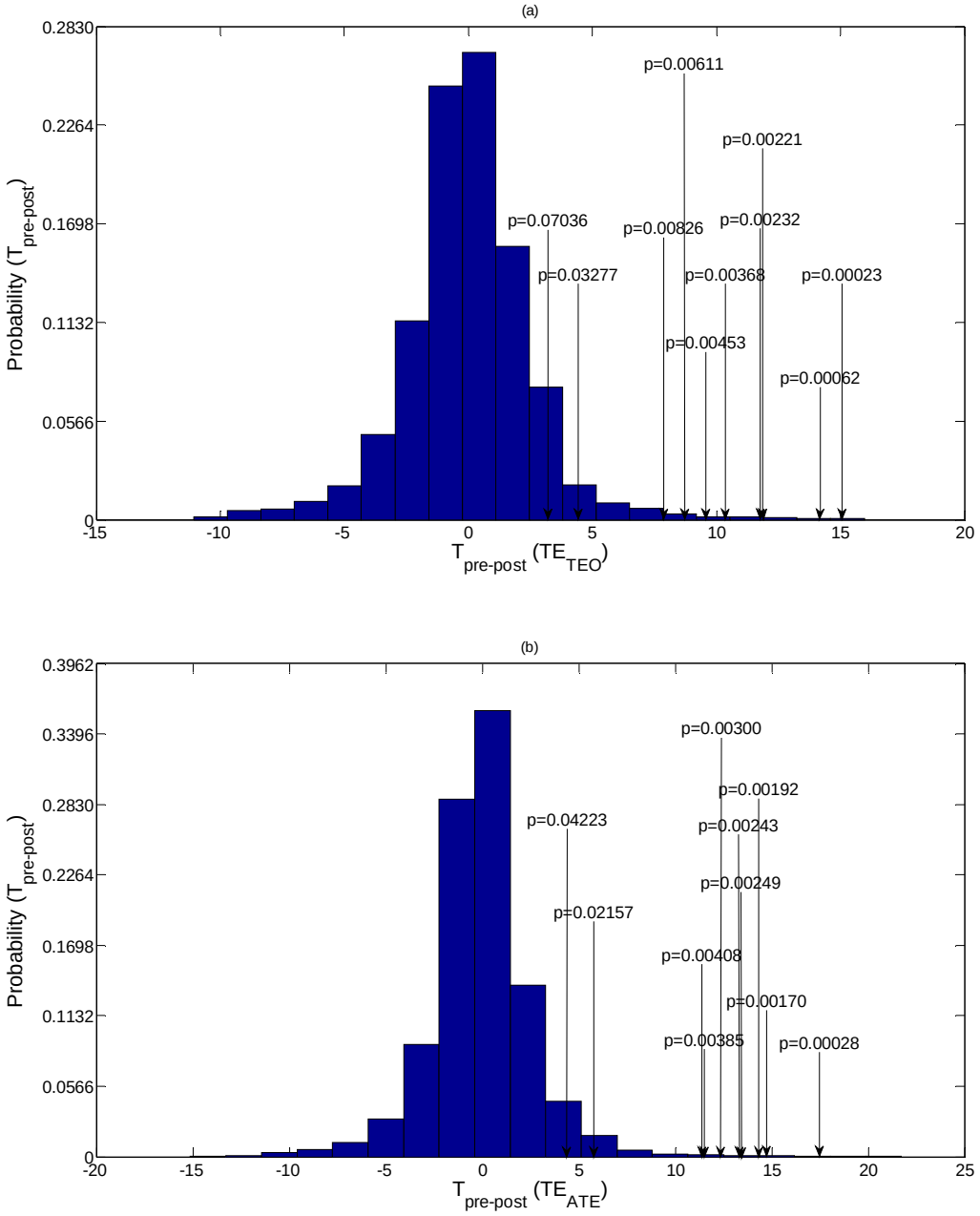

Figure 5.7. (a) and (b) show the p value at seizures for TEO_{RTD} and ATE_{RTD} respectively.

It is important to note that these observations can be made with even smaller duration of EEG data, but to rule out possibly large effects of short artifacts and small sample bias, and to test for consistency, we considered long durations.

These observations herein are promising for their employment in the solution of the problem of focus localization from interictal periods. This topic is further discussed in the next section. Table 5.1 below shows the p-value at seizures for patient 1.

Table 5.1. p-values from the t-test $T_{pre-post}$ for RTD6 per seizure (patient 1).

Seizure number	p-values ($\boldsymbol{ATE_{RTD6}}$)	p-values ($\boldsymbol{TEO_{RTD6}}$)
Seizure 1	0.0003	0.0006
Seizure 2	0.0017	0.0023
Seizure 3	0.0041	0.0061
Seizure 4	0.0216	0.0328
Seizure 5	0.0025	0.0083
Seizure 6	0.0024	0.0045
Seizure 7	0.0030	0.0037
Seizure 8	0.0019	0.0002
Seizure 9	0.0038	0.0022
Seizure 10	0.0422	0.0704

5.5. Information Flow in Interictal EEG

The 4 measures of information flow were calculated for interictal periods (without any seizures) too. Figure 5.8 shows the plot for TEO_i, TEI_i, $TEN_i$and ATE_i for 24 hour interictal EEG (void of seizures).

Description of plots

For each of the 4 methods (TEO, TEI, TEN and ATE), corresponding color plots were generated for each measure across time and electrode space. Horizontal

axis is time duration and the vertical axis has the montage with labeled electrodes. The color bar on the side of the plots codes for the values of each measure. The red end of the spectrum denotes higher measure values and the blue end of the spectrum denotes lower values. In Figure 5.8 (a) we observe red color for RTD6 over time. This indicates that RTD6 has higher outflow of information (TEO) compared to other sites which have colors of lower intensity.

Observations

1) $TEO,$ the outflow from each electrode in the plots, shows higher values at RTD4, RTD6 (clinically assessed focal sites) throughout the interictal period supporting the hypothesis that focus is a driver for normal brain sites even interictally.
2) TEI, estimated as the maximum inflow to each electrode in the plots, shows higher values in RTD2, RTD4 throughout the interictal period. This, along with the observation in (1) above, supports the hypothesis that focus also behaviors as an information sink in both of these patients.
3) The above two observations motivated us to look into measures of net driving strength and coupling strength. TEN , which quantifies the net driving strength as described in Equation 3.16, shows the highest driving strength in RTD6 over time compared to the rest of the electrode sites.
4) Finally, , which quantifies the coupling strength between sites, shows the highest values at the entire right temporal region. This implies that RTD region has the stronger connections than any other region in the brain in both patients.

(a)

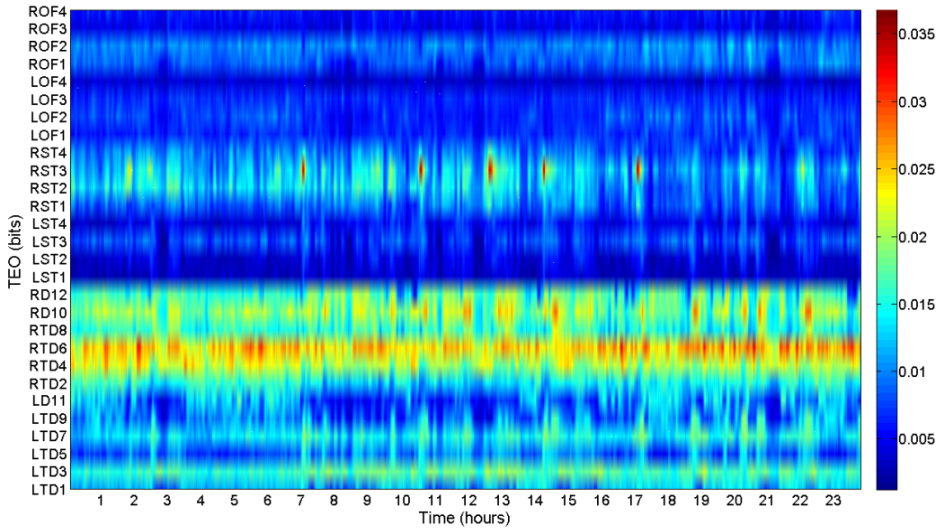

(b)

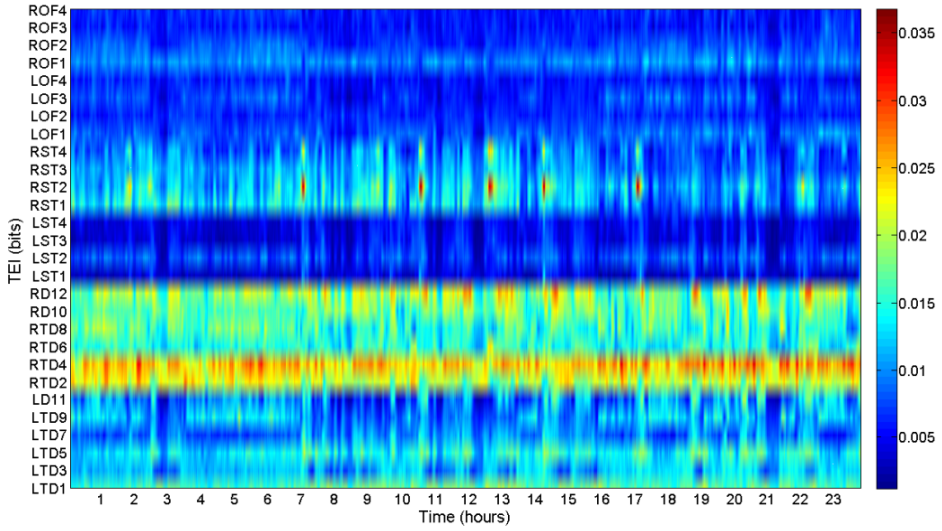

Figure 5.8. Patient 1: (a) $TEO_i \; \forall \; i$ vs. time. (b) Similar plot for I_i .

(a)

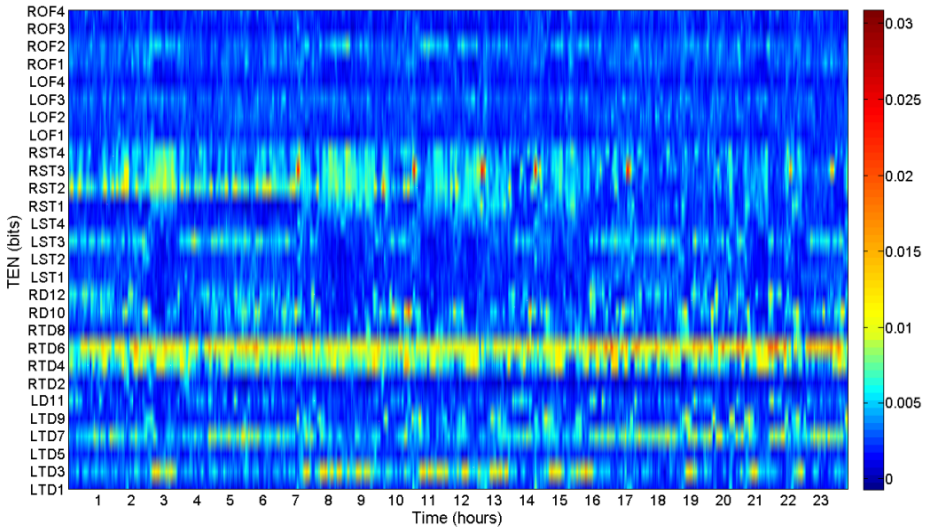

(b)

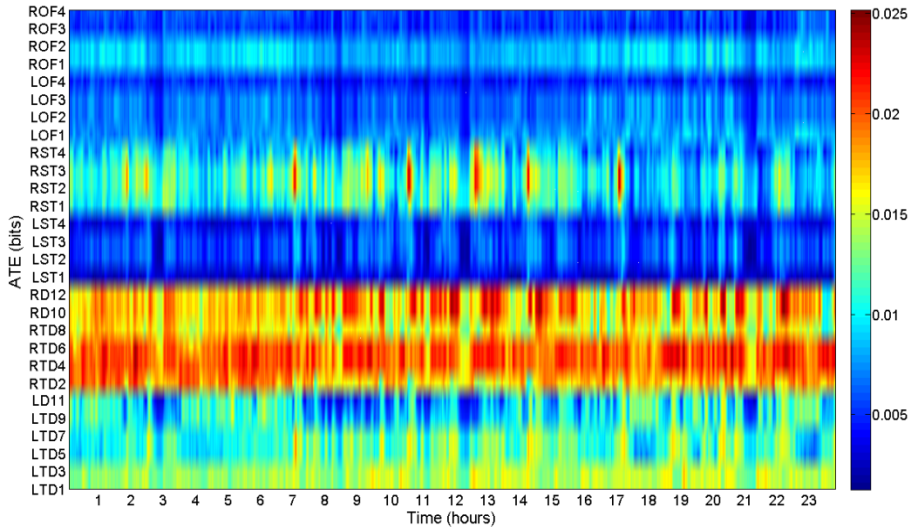

Figure 5.9. Patient 1: (a) $TEO_i \; \forall \; i$ vs. time. (b) Similar plot for TEI_i.

(a)

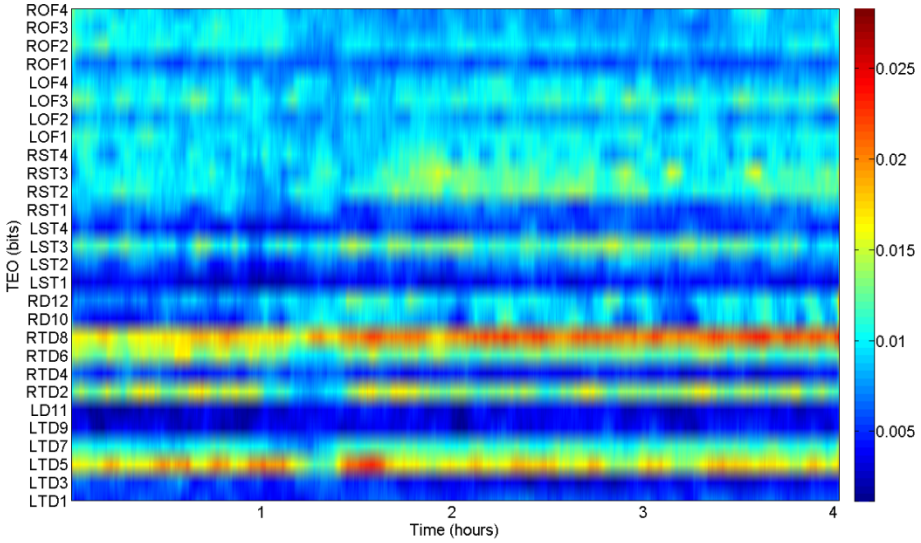

(b)

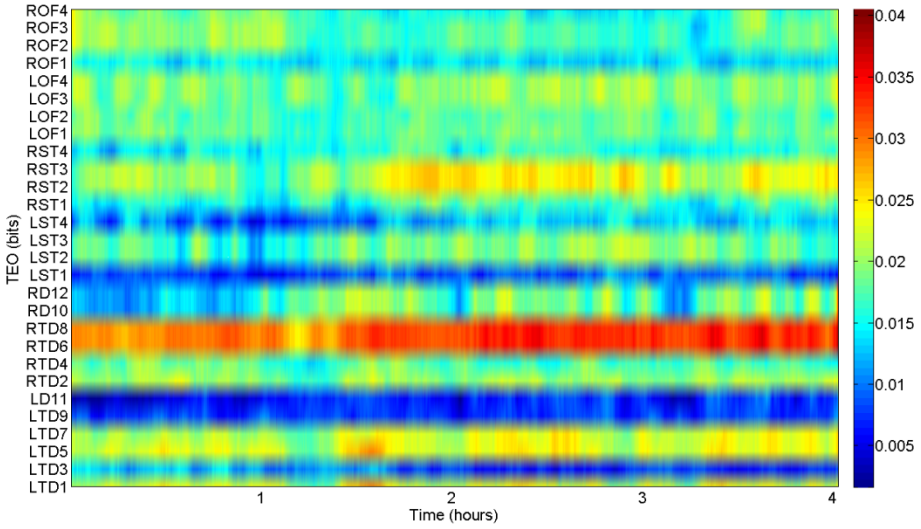

Figure 5.10. Patient 2: (a) $TEO_i \; \forall \; i$ vs. time. (b) Similar plot for TEI_i.

5.6. Application of TE to Epileptogenic Focus Localization

In this section we present the results from the analysis of the EEG from both of our patients by the average value of the four information flow measures we developed. We already noticed in section 5.5 that the focus shows maximum outflow and inflow, and maximum coupling strength of all other electrodes. In

order to be able to successfully localize the focus, we venture out to find the site with highest TEO. TEO is able to detect the exact site with the highest outflow that might correspond to our hypothesis that focus drives the neighboring sites.

In some patient cases it is hard to localize the focus exactly due to changing dynamics of the focal sites over time and/or inability to record from the focus due to inadequate electrode placement. The clinically assessed focus for Patient 1 was RTD4 and RTD6. TEO is able to specifically show RTD6 as the site with highest outflow. Our analysis showed that TEO might be a better measure to detect a specific site than a region.

As mentioned in section 5.1, clinical assessment is amenable to errors with regard to localizing to a particular electrode site (e.g., RTD6) compared to localizing to a region (e.g., RTD). This may be attributed to the fact that an epileptogenic focus may be present at a location neighboring and not exactly at a recording electrode site. It was noticed that the use of ATE gave results closer to the clinical assessment for both of our patients (RTD4 and RTD6). This may be because ATE mainly detects maximum coupling amongst sites, that is, it detects sites with maximum information flow in both directions. This could prove useful also in focus *lateralization,* that is, where even the location of the focus within a hemisphere of the brain cannot be identified. Figure 5.9 shows bar plots of average over time TEO per electrode site for the same duration as in Figure 5.4 and 5.5 in patient 1. We can clearly observe that RTD6 (focus) exhibits the maximum outflow of all other sites (we observed the same finding in Figures 5.4 and 5.5 visually but did not quantify it). Figure 5.10 shows the corresponding plots for patient 2.

(a)

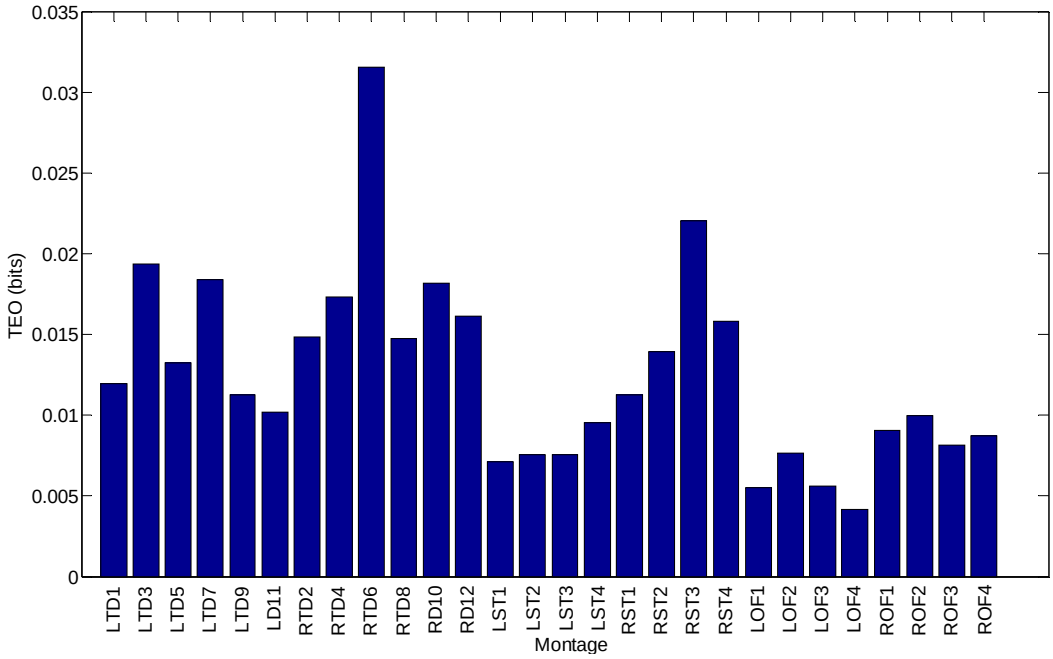

(b)

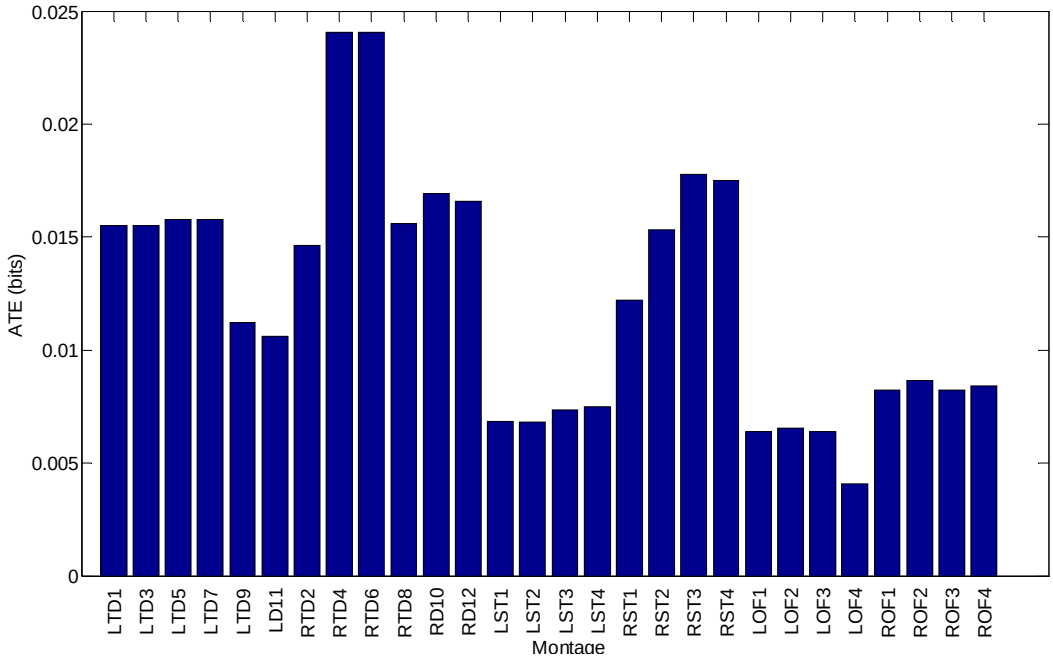

Figure 5.11. Patient 1: Bar plot for the time averaged values of (a) $TEO_i \forall\, i$. (b) $ATE_i \forall\, i$. RTD6 shows the highest values for TEO and RTD4 and RTD6 show the highest values ATE, which match the clinical assessment of focus location.

(a)

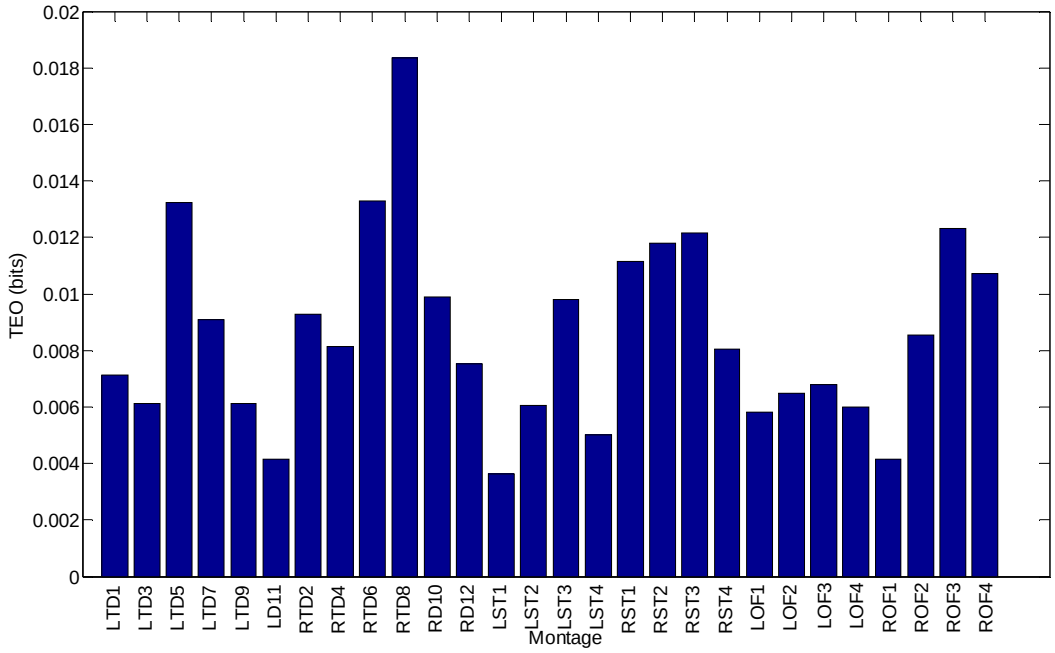

(b)

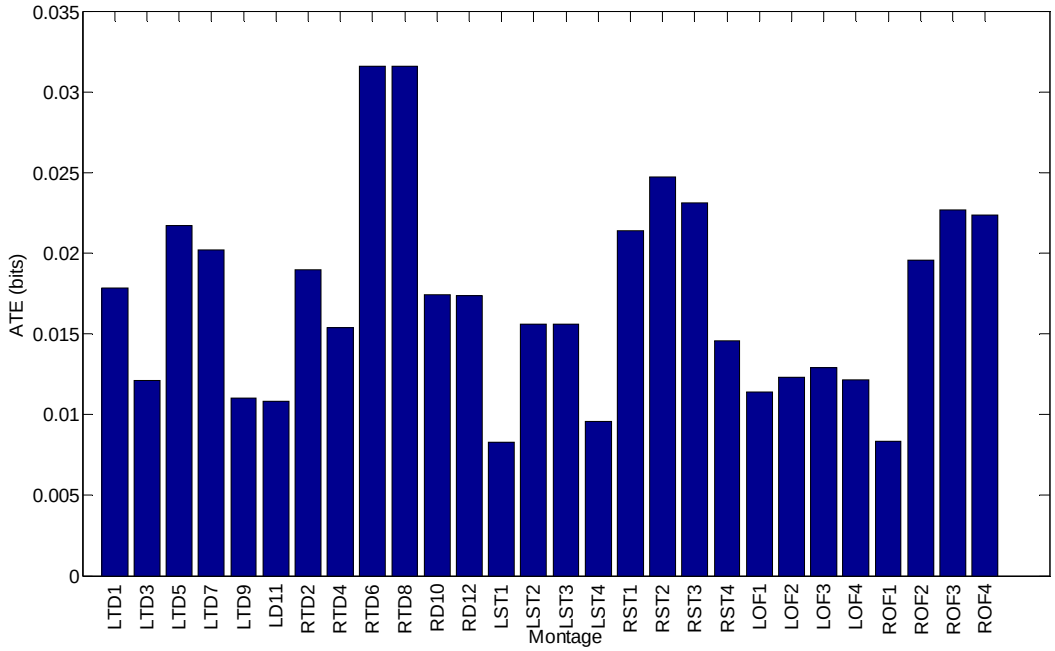

Figure 5.12. Patient 2: Bar plot for the time averaged values of (a) $TEO_i \forall i$. (b) $ATE_i \forall i$. RTD6 shows the highest values for TEO and RTD4 and RTD6 show the highest values ATE, which match the clinical assessment of focus location.

Table 5.2. Epileptogenic focus localization: Comparison of different methods of information flow localization techniques with clinical assessment of focus location

Patient ID	Focus (Clinical Assessment: All Seizures)	Focus Localization (TEO)	Focus Localization (ATE)
Patient 1	RTD2, RTD4, RTD6	RTD6	RTD4, RTD6
Patient 2	RTD2, RTD4, RTD6, RTD8	RTD8	RTD6, RTD8

Table 5.2 shows the results obtained from our methods for focus location compared to clinical assessment. The clinical reports, by visual inspection of the EEG at seizures' onset, show different localization for each seizure and an overall localization to RTD. The clinical results shown in the Table represent an agreement across all seizures analyzed. A more extensive analysis across several patients and development of a robust focus localization algorithm is left for future work.

5.7. Application to Seizure Dynamics, Seizure Prediction and Seizure Detection

Sections 5.3 to 5.6 showed that our developed TE-based measures of information flow provide new insights into understanding the dynamics of EEG preictally and postictally across two patients. These methods can be extended to achieve a robust framework for Focus Localization (Section 5.5 and 5.6) and Seizure Detection (TEO_{FOCUS}, Section 5.4). Once Focus Localization is achieved

from the interictal period, TEO_{FOCUS} can be used for seizure detection by observing the change in information pre to post ictally (statistically shown in Section 5.4).

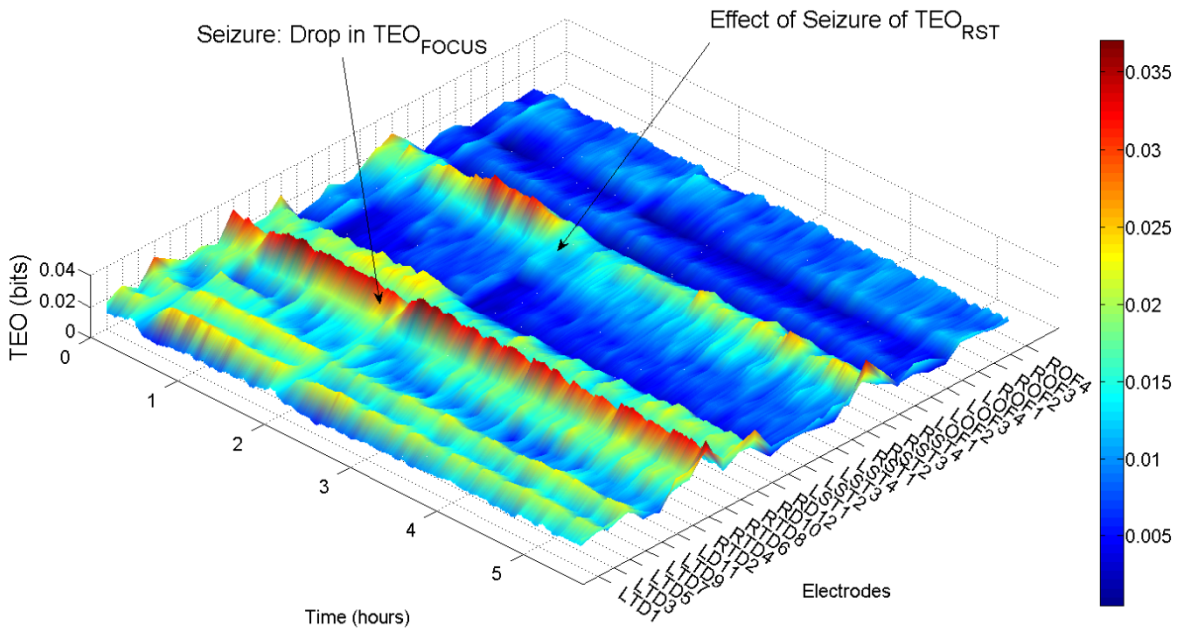

Figure 5.13. Patient 1: $TEO_i \forall\ i$ over time shows breakage of information flow at seizure across all channels. (Smoothened for visualization.)

Change in information dynamics due to an upcoming seizure can be observed temporally and spatially in Figure 5.11. It is interesting to observe the different dynamical behavior of each channel. TEO_{RTD} drops in value immediately after seizure but resumes its preictal value in a very short period. This behavior of the focus was observed consistently at all seizures. On the other hand, TEO_{RST} behaves differently. The drop in TEO_{RST} is observed long term and its value remains low for several hours after a seizure before it increases in value.

Figure 5.12 (a) shows a similar plot for a different tape in patient 1. We can see that there is breakage of information flow (TEO) across all channels during

seizure. Figure 5.12 (b) shows the plot of TEO_{RTD6} and we observe the drop right at seizure. This phenomenon is not visible in Figure 5.12 (c) for O_{LST2} , where its values are very low. The application of TE and TE-based methods shown in this chapter opens a window to the understanding of the dynamics of seizures and their implications, a very less understood topic to date.

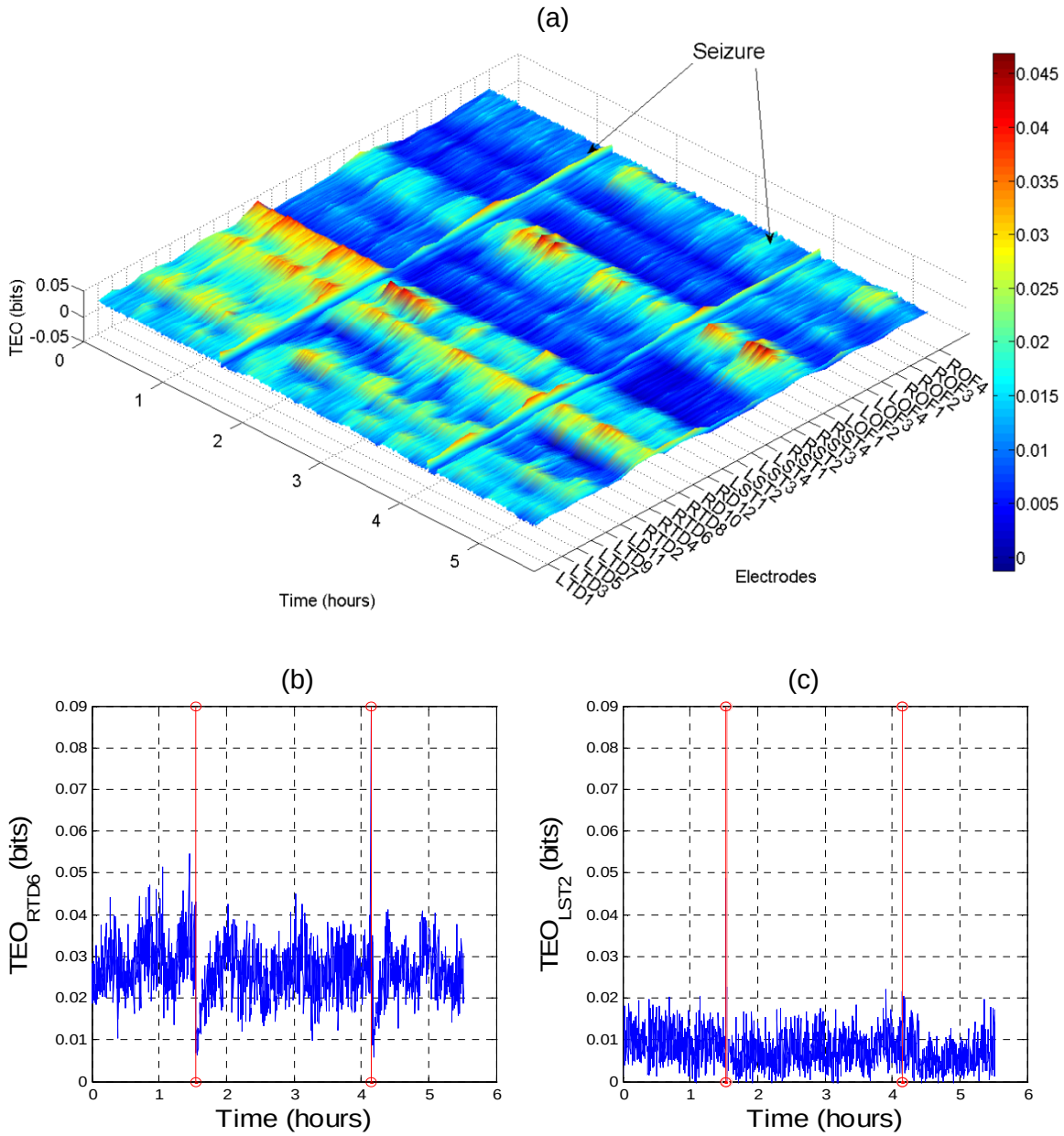

Figure 5.14. Patient 1: (a) $TEO_i \forall\, i$ over time shows the breakage of information flow per site at seizures. (Smoothened for visualization.) (b) same plot for TEO_{RTD6} (c) same plot for TEO_{LST2} . Red lines indicate the occurrence of seizures.

Chapter 6

CONCLUSION

One of the objectives of this thesis was to address the underlying mechanisms of epilepsy as a dynamical disorder through the study of Information Flow in the epileptic brain.

At first, a new framework was developed to analyze Information flow in complex network of coupled sub-systems using Transfer Entropy and derived measures. The application of the methods on model data was successful in distinguishing the desired sub-subsystem from the whole system, with respect to its interactions with other sub-systems. The simulation results and analysis also showed the robustness of these methods to noise. Visual results were provided to help clearly identify the relative behavior of each sub-system.

After validating the efforts on the models, the methods were applied to long-term EEG data from two patients with focal epilepsy. Several observations were made by analyzing the EEG under the assumption that brain consists of highly complex coupled subsystems. The analysis was performed separately in interictal and ictal periods for the two patients. The results from the analysis in the interictal periods showed that the epileptic focus had maximum outflow in information throughput. This supports the hypothesis that the focus is a driver to the neighboring response systems (brain sites). Results regarding strength of coupling support the hypothesis that focus has the strongest interaction with neighboring sites with respect to inflow and outflow of information.

The analysis of EEG from the ictal period sheds light on the dynamics of the transition to seizures (ictal periods) and the mechanisms involved. The results showed that seizures behave as deterrents for connection of the focus

with the rest of the brain. A drop in information flow from the focus is observed postictally. While the focal sites recover immediately and continue to be the strongest driver, other sites take time to restore their information flow. We believe that this observation opens the door to the development of important tools for both seizure detection and focus localization. The statistical results we herein obtained along these directions provide very good supporting evidence towards these two goals. There also exists the opportunity for possible application of such results to improvement of seizure prediction algorithms.

In summary, the tools developed and the results generated within this thesis hold promise for enhancement of new concepts in the fields of seizure prediction, seizure detection and focus localization, and provide a new framework for engineering studies and discoveries in epilepsy. Future work should use these tools to further investigate the mechanisms of epileptogenesis and ictogenesis, as well as the workings of the normal brain.

REFERENCES

Abarbanel, H. D. I. (1996). *Analysis of observed chaotic data* Springer Verlag.

Asano, E., Pawlak, C., Shah, A., Shah, J., Luat, A. F., Ahn-Ewing, J., & Chugani, H. T. (2005). The diagnostic value of initial video-EEG monitoring in children--review of 1000 cases. *Epilepsy Research, 66*(1-3), 129-135.

Bentley, J. L., & Friedman, J. H. (1979). Data structures for range searching. *ACM Computing Surveys (CSUR), 11*(4), 397-409.

Bharucha-Reid, A. T. (1997). *Elements of the theory of markov processes and their applications* Dover Pubns.

Cormen, T. H. (2001). *Introduction to algorithms* The MIT press.

Dudek, F. E., & Spitz, M. (1997). Hypothetical mechanisms for the cellular and neurophysiologic basis of secondary epileptogenesis: Proposed role of synaptic reorganization. *Journal of Clinical Neurophysiology, 14*(2), 90.

Eastman, S. (1982). Tree structures for high dimensionality nearest neighbor searching. *Information Systems, 7*(2), 115-122.

Engel Jr, J., Van Ness, P., Rasmussen, T., & Ojemann, L. (1993). Outcome with respect to epileptic seizures. *Surgical Treatment of the Epilepsies, 2*, 609-621.

Engel, J., Pedley, T. A., & Aicardi, J. (2008). *Epilepsy: A comprehensive textbook* Lippincott Williams & Wilkins.

Feldmann, U., & Bhattacharya, J. (2004). Predictability improvement as an asymmetrical measure of interdependence in bivariate time series. *International Journal of Bifurcation and Chaos, 14*(2), 505-514.

Fraser, A. M., & Swinney, H. L. (1986). Independent coordinates for strange attractors from mutual information. *Physical Review A, 33*(2), 1134.

Friedman, J. H., Baskett, F., & Shustek, L. J. (1975). An algorithm for finding nearest neighbors. *Computers, IEEE Transactions on, 100*(10), 1000-1006.

Friedman, J. H., Bentley, J. L., & Finkel, R. A. (1977). An algorithm for finding best matches in logarithmic expected time. *ACM Transactions on Mathematical Software (TOMS), 3*(3), 209-226.

Geweke, J. (1982). Measurement of linear dependence and feedback between multiple time series. *Journal of the American Statistical Association, 77*(378), 304-313.

Goldstein, M., & Harden, C. (2000). Continuing exploration of the neuropsychiatry of seizures: A review of anxiety and epilepsy. *Epilepsy Behav, 1*, 228-234.

Gotman, J., Gloor, P., & Ives, J. R. (1985). *Long-term monitoring in epilepsy* Elsevier New York, NY, USA: Sole distributors for the USA and Canada, Elsevier Science Pub. Co., Amsterdam; New York.

Granger, C. W. J. (1969). Investigating causal relations by econometric models and cross-spectral methods. *Econometrica: Journal of the Econometric Society,* , 424-438.

Hénon, M. (1976). A two-dimensional mapping with a strange attractor. *Communications in Mathematical Physics, 50*(1), 69-77.

Hlavackova-Schindler, K., Palus, M., Vejmelka, M., & Bhattacharya, J. (2007). Causality detection based on information-theoretic approaches in time series analysis. *Physics Reports, 441*(1), 1-46.

Iasemidis, L. D., Chris Sackellares, J., Zaveri, H. P., & Williams, W. J. (1990). Phase space topography and the lyapunov exponent of electrocorticograms in partial seizures. *Brain Topography, 2*(3), 187-201.

Iasemidis, L. D., Shiau, D. S., Chaovalitwongse, W., Sackellares, J. C., Pardalos, P. M., Principe, J. C., . . . Tsakalis, K. (2003). Adaptive epileptic seizure prediction system. *Biomedical Engineering, IEEE Transactions on, 50*(5), 616-627.

Iasemidis, L., & Sackellares, J. (1991). The temporal evolution of the largest lyapunov exponent on the human epileptic cortex. *Measuring Chaos in the Human Brain,* , 49–82.

Kaminski, M., & Blinowska, K. (1991). A new method of the description of the information flow in the brain structures. *Biological Cybernetics, 65*(3), 203-210.

Kantz, H., Schreiber, T., & Mackay, R. S. (1997). *Nonlinear time series analysis* Cambridge University Press Cambridge:.

Kennel, M. B., Brown, R., & Abarbanel, H. D. I. (1992). Determining embedding dimension for phase-space reconstruction using a geometrical construction. *Physical Review A, 45*(6), 3403.

Koblar, S. A., Black, A. B., & Schapel, G. J. (1992). Video-audio/EEG monitoring in epilepsy--the queen elizabeth hospital experience. *Clinical and Experimental Neurology, 29*, 70-73.

Kwan, P., & Brodie, M. J. (2000). Early identification of refractory epilepsy. *The New England Journal of Medicine, 342*(5), 314-319.

Lee, D. T., & Wong, C. (1977). Worst-case analysis for region and partial region searches in multidimensional binary search trees and balanced quad trees. *Acta Informatica, 9*(1), 23-29.

Liang, H., Ding, M., & Bressler, S. L. (2001). Temporal dynamics of information flow in the cerebral cortex. *Neurocomputing, 38*, 1429-1435.

Loiseau, J., Loiseau, P., Guyot, M., Duche, B., Dartigues, J. F., & Aublet, B. (1990). Survey of seizure disorders in the french southwest. I. incidence of epileptic syndromes. *Epilepsia, 31*(4), 391-396.

Lopes da Silva, F. H., & Pijn, J. P. (1995). Epilepsy: Network models of generation. *The Handbook of Brain Theory and Neural Networks,* , 367-369.

Manford, M., Hart, Y. M., Sander, J. W., & Shorvon, S. D. (1992). National general practice study of epilepsy (NGPSE): Partial seizure patterns in a general population. *Neurology, 42*(10), 1911-1917.

Mormann, F., Kreuz, T., Andrzejak, R. G., David, P., Lehnertz, K., & Elger, C. E. (2003). Epileptic seizures are preceded by a decrease in synchronization. *Epilepsy Research, 53*(3), 173-185.

Ott, E. (2002). *Chaos in dynamical systems* Cambridge Univ Pr.

Paluš, M., Komárek, V., Hrnčíř, Z., & Štěrbová, K. (2001). Synchronization as adjustment of information rates: Detection from bivariate time series. *Physical Review E, 63*(4), 046211.

Paulus, M., Komarek, V., Prochazka, T., Hrncir, Z., & Sterbova, K. (2001). Synchronization and information flow in EEGs of epileptic patients. *Engineering in Medicine and Biology Magazine, IEEE, 20*(5), 65-71.

Priestley, M. B. (1981). Spectral analysis and time series.

Quiroga, R. Q., Arnhold, J., Lehnertz, K., & Grassberger, P. (2000). Kulback-leibler and renormalized entropies: Applications to electroencephalograms of epilepsy patients. *Physical Review E, 62*(6), 8380.

Rapp, P., Albano, A., & Mees, A. (1988). Calculation of correlation dimensions from experimental data: Progress and problems. *Dynamic Patterns in Complex Systems.World Scientific,* , 191-205.

Rosenblum, M. G., & Pikovsky, A. S.Detecting direction of coupling in interacting oscillators. *PHYSICAL REVIEW E Phys Rev E, 64*, 045202.

Rössler, O. E. (1976). An equation for continuous chaos. *Physics Letters A, 57*(5), 397-398.

Schiff, S. J., So, P., Chang, T., Burke, R. E., & Sauer, T. (1996). Detecting dynamical interdependence and generalized synchrony through mutual prediction in a neural ensemble. *Physical Review E, 54*(6), 6708.

Schiller, Y., & Najjar, Y. (2008). Quantifying the response to antiepileptic drugs. *Neurology, 70*(1), 54.

Schreiber, T. (2000). Measuring information transfer. *Physical Review Letters, 85*(2), 461-464.

Smirnov, D. A., & Bezruchko, B. P. (2003). Estimation of interaction strength and direction from short and noisy time series. *Physical Review E, 68*(4), 046209.

Smith, R. L., Wigley, T. M. L., & Santer, B. D. (2003). A bivariate time series approach to anthropogenic trend detection in hemispheric mean temperatures. *Journal of Climate, 16*(8), 1228-1240.

Takens, F. (1981). Detecting strange attractors in turbulence. *Dynamical Systems and Turbulence, Warwick 1980,* , 366-381.

Theiler, J. (1986). Spurious dimension from correlation algorithms applied to limited time-series data. *Physical Review A, 34*(3), 2427.

Wiener, N. (1956). Modern mathematics for engineers.

Williams, G. P. (1997). *Chaos theory tamed* CRC Press.